Technische Universität Ilmenau

Fakultät für Mathematik und Naturwissenschaften

Masterstudiengang Technische Physik

Institut für Physik

Fachgebiet Theoretische Physik II

One-dimensional hopping transport with nearest-neighbor interactions

vorgelegt von

Marcel Dierl

Betreuer: Dr. Mario Einax

Masterarbeit

2010

Abstract

In thermal equilibrium, the probability to be in a certain microstate is given by the Gibbs-Boltzmann distribution, but this is more an exceptional case in nature. Especially all living organisms are driven or they are exposed to external driving forces. Consequently, the equilibrium statistical ensembles cannot be applied. In order to study physical properties of complex systems far from equilibrium, mainly simple model systems like driven lattice gases are used. In particular, for one-dimensional lattice gases with hard-core repulsion several analytical methods are known, leading to exact results. However, these approaches fail for systems with additional particle-particle interactions.

In the present thesis, it is shown how such systems can be calculated by the classical density functional theory (DFT) together with the local equilibrium approximation. The basic idea consists in describing non-equilibrium states by equilibrium distributions and rewriting occurring density correlators in terms of one-particle densities. As a result, macroscopic quantities like currents are accessible in an analytical form and solvable kinetic equations can be derived from the underlying master equation. Based on the concept of DFT, an extension to a time-dependent theory (TDFT) allows the characterization of dynamic processes like the time evolution of density profiles. The TDFT findings are tested against kinetic Monte Carlo simulations. Both the analysis of the current and the investigation of density profiles show an excellent agreement between theory and numerical experiments.

Keywords: driven lattice gases, nearest-neighbor interactions, density correlations, classical density functional theory

Zusammenfassung

Im thermischen Gleichgewicht ist die Wahrscheinlichkeit, ein System in einem bestimmten Zustand vorzufinden, durch die Gibbs-Boltzmann-Verteilung gegeben. Allerdings ist dieser Fall in der Natur eher die Ausnahme. Insbesondere sind alle lebenden Organismen angetrieben oder äußeren Triebkräften ausgesetzt. Die statistischen Ensembles des Gleichgewichts sind diesbezüglich nicht mehr anwendbar. Um physikalische Eigenschaften von komplexen Systemen fernab vom thermischen Gleichgewicht zu studieren, wird im großen Maße auf einfache Modellsysteme, wie getriebene Gittergase, zurückgegriffen. Speziell für eindimensionale Gittergase mit Hard-Core-Wechselwirkungen existiert eine Vielzahl analytischer Lösungsmethoden, die zu exakten Resultaten führen. Jedoch versagen diese Verfahren bei der Einführung von zusätzlichen Teilchen-Teilchen-Wechselwirkungen.

In der vorliegenden Arbeit wird gezeigt, wie mittels klassischer Dichtefunktionaltheorie (DFT) und der Idee des lokalen Gleichgewichts dennoch eine Analyse jener Systeme möglich ist. Hierbei werden Nichtgleichgewichtszustände durch Gleichgewichtsverteilungen approximativ beschrieben und auftretende Dichtekorrelationen werden im Sinne der DFT als reine Funktionen von Einteilchendichten ausgedrückt. Dadurch sind makroskopische Größen, wie Ströme, analytisch beschreibbar und lösbare kinetische Gleichungen können aus der entsprechenden Mastergleichung abgeleitet werden. Ausgehend von den Resultaten der DFT ist durch die Erweiterung zur zeitabhängigen Theorie (TDFT) auch die Charakterisierung dynamischer Prozesse, wie die zeitliche Entwicklung von Dichteprofilen, möglich. Die Ergebnisse der TDFT werden mit kinetischen Monte Carlo Simulationen evaluiert. Sowohl die Stromanalyse als auch die Untersuchung der Dichteprofile lassen hierbei eine sehr gute quantitative Übereinstimmung zwischen Theorie und numerischen Experimenten erkennen.

Schlagwörter: getriebene Gittergase, Nächste-Nachbar-Wechselwirkungen, Dichtekorrelationen, klassische Dichtefunktionaltheorie

Contents

List of Figures

Chapter 1

Introduction

Transport processes in low-dimensional nanostructures are of great importance for current applications in physics, biology and materials science. In this context, the focus lies on classical systems far from equilibrium. Investigations of effectively one-dimensional structures, which are also existent in nature, already permit a deep understanding of transport mechanisms. Famous examples of such biological processes are the motion of motor proteins along a microtubule or an actin track, the protein synthesis by which the ribosome reads the sequence of the mRNA, ions diffusing in narrow channels or the movement of ants on trails. Current research is concerned with the development of theoretical model approaches which describe and characterize these systems. Promising methods are based on hopping models that are coupled to particle reservoirs at the system boundaries.

Due to a lacking physical connection, most hopping models are characterized by only hard-core repulsion that merely prevents multiple occupations on a lattice site. For such systems, several analytical methods like matrix approach or Bethe ansatz are known, leading to an exact distribution of microstates (for review, see [Der98, Sch00, GM06, BE07], and references therein). An analogy to these lattice models may be made by considering the ideal gas in which no intermolecular forces occur. Deviations from ideality result from interactions of gas molecules, captured by the van der Waals equation. In the same spirit, it is interesting to study the influence of particle-particle interactions on the dynamics of driven systems. To this end, a one-dimensional lattice gas is used in which particles are seen as hard spheres interacting with their nearest neighbors.

Taking into account particle-particle interactions, the mentioned analytical techniques cannot be applied straightforwardly. Moreover, a simple factorization ansatz for particle-particle correlations does not yield the desired non-equilibrium properties. A slightly improved mean-field approach is given by a field-theoretical description based on the Landau-Ginzburg theory [LSZ89]. By contrast, models proposed in Ref. [KLS84] investigate steady-state properties from an equilibrium distribution of the Ising model. This idea is used in several works for studying the current behavior and kinetics of phase transformations in driven lattice gases [Kru91, PS99, HKPS01].

The important goal of these studies has been to show that interparticle interactions lead to intriguing results in non-equilibrium physics. In view of driven systems which cannot be described by this method, no satisfactory analytical technique is available up to now. The roots of the stepmotherly treatment of systems with additional particle-particle interactions lie in a fast increasing complexity of corresponding analytical calculations. As a consequence, numerical studies are preferred, whereby a deep insight into transport mechanisms fails to be achieved. It is thus desirable to develop an analytical concept dealing with interparticle interactions.

The goals of this work are twofold. First, an analytical method for an optimal characterization of one-dimensional lattice gases with nearest-neighbor coupling is developed. In particular, the current-density relation and kinetics of density profiles are discussed by use of this concept. The second goal is to verify the method by corresponding numerical experiments. The present thesis focuses on the totally asymmetric simple exclusion process (TASEP), which has been of considerable interest within the physics community as a prototypical model of non-equilibrium behavior. This model is based on a one-dimensional lattice in which particles update their states through hard-core exclusion and move unidirectionally. In this work, the usual form of the TASEP is extended by nearest-neighbor interactions. Hopping rates, being functions of local particle configurations, take this property into account.

A powerful analytical technique for interacting lattice systems is the classical density functional theory (DFT) based on a local equilibrium approximation. The basic idea consists in rewriting correlators as functions of one-particle densities. This thesis shows that essential properties of the one-dimensional transport model, suggested here, are accessible at all times using the time-dependent variant of DFT, called TDFT. At long times, the TDFT approach yields the current-density relation and steady-state density profiles. Analytical findings are tested against continuous-time Monte Carlo simulations.

The structure of this work is as follows: Chapter 2 provides the reader with an introduction to one-dimensional driven lattice gases. Not only the basic idea and various models are presented, but also answers to questions concerning integrability and expandability of these systems are given. Chapter 2 concludes with a generalized TASEP, where particles are allowed to interact with their neighboring environment on top of the pure hard-core repulsion. After defining the model, Chapter 3 pays attention to methods and tools for studying such lattice gases. In particular, it is shown how the DFT technique can be applied to driven systems with particle-particle interactions and how this approach can be verified numerically. Afterwards, Chapter 4 deals with a TDFT discussion of systems which are imposed by periodic and open boundary conditions. This thesis concludes with Chapter 5 which contains a summary of basic results and an outlook on open questions and prospective studies.

Chapter 2

A guide to driven lattice gas models

This chapter is concerned with the so-called simple exclusion process, a one-dimensional lattice model of hopping particles with at most one particle at each site. Due to the importance of non-equilibrium behavior in biology, physics, economy, in the social science or even in everyday life, the enormous relevance of such a system for fundamental research is justified in the first section. The second section reviews the simple exclusion process and its solutions derived by several approaches. Since this academic system is not able to explain challenging physical phenomena, extensions of the already existing model are needed. Hence, this chapter concludes with two modified concepts, one uses the example of traffic and the other includes systems with repulsive nearest-neighbor interactions.

2.1 Statistical physics out of equilibrium

Statistical mechanics provides a framework to relate microscopic properties of individual particles in a classical system to macroscopic state variables like pressure or macroscopic currents. As a particular subclass of stationary macrostates, equilibrium states are in general characterized by time-independent and spatially homogeneous macroscopic observables. Another distinctive property of equilibrium states is the absence of macroscopic currents.

Isolated equilibrium systems correspond to the microcanonical ensemble[1]. In these systems, the number of particles, the volume and also the energy are conserved. The probability to find such a system in a certain microstate just reads $1/\Omega$, where Ω is the number of all possible microstates consistent with a given macrostate. A system, which is coupled to a heat reservoir in such a manner that the system is kept at constant temperature and the average energy is conserved, belongs to the canonical ensemble. For that, a probability distribution of microscopic states is also known, called Gibbs-Boltzmann distribution. More precisely, the probability $P_{\mathrm{eq}}(\mathbf{n})$

[1]Ensembles in thermodynamics include every possible microstate a system could be in.

of a fixed configuration $\mathbf{n}$ with energy $\mathcal{H}(\mathbf{n})$ is given by

$$P_{\mathrm{eq}}(\mathbf{n}) = Z^{-1}\,\mathrm{e}^{-\beta\mathcal{H}(\mathbf{n})}, \tag{2.1}$$

where β is the inverse thermal energy and Z denotes the partition function. If the number of particles is not fixed, i.e., a particle flux between system and environment is allowed, one introduces the grand canonical ensemble. Here, particle and energy fluctuations are associated with the chemical potential μ.

To summarize, there is a thermodynamic theory to describe the complete stochastic behavior of equilibrium systems. In contrast to this, today's literature does not deal with a general theory that characterizes the whole process of non-equilibrium systems. Nevertheless, some approaches close to equilibrium exist, such as the Green-Kubo relation, Kramers-Kronig theory or Onsager's relation. Even far from equilibrium, Jarzynski extracts equilibrium information from an ensemble of non-equilibrium measurements [Jar97]. However, systems in non-equilibrium stationary states are not well understood, certainly not with the power of those that are in equilibrium.

Non-equilibrium processes play an important role in life of organisms. For instance, the intracellular transport is ensured by diffusion mechanisms [MS08]. Such processes are called boundary-driven processes since the non-equilibrium behavior is generated by open boundary conditions. In these systems, the non-vanishing mass current is proportional to the concentration gradient, known as Fick's first law. The stationary state, also referred to as steady state, is characterized by a time-independent current. Beside boundary-driven systems, one hits upon bulk-driven processes which may also have the property of stationarity. A bulk driven process is given by the example of Ohm's law describing electron movement caused by an electric field. However, non-equilibrium processes can also be observed in fields having, at first glance, a non-physical background. As an example, consider the stock market, where price fluctuations in speculative market dynamics show interesting non-equilibrium properties [PS07].

Various stochastic processes are Markovian ones that are formulated by the master equation [Gil92]. The master equation describes the time evolution of the probability $P(\mathbf{n}, t)$ of a system to be in a microstate $\mathbf{n}$ at time t,

$$\frac{\partial}{\partial t}P(\mathbf{n}, t) = \sum_{\mathbf{n}'}\left[\Gamma_{\mathbf{n}'\to\mathbf{n}}P(\mathbf{n}', t) - \Gamma_{\mathbf{n}\to\mathbf{n}'}P(\mathbf{n}, t)\right]. \tag{2.2}$$

The right-hand side of Eq. (2.2) corresponds to the change of the probability $P(\mathbf{n}, t)$ in time, which is composed of a gain term with rate $\Gamma_{\mathbf{n}'\to\mathbf{n}}$ controlling a transition from $\mathbf{n}'$ to $\mathbf{n}$ and a corresponding loss term with transition rate $\Gamma_{\mathbf{n}\to\mathbf{n}'}$. Note that the term $\mathbf{n}' = \mathbf{n}$ does not appear in the summation.

Frequently, stationary solutions of the master equation are of particular importance. In order to find such solutions, the left-hand side of (2.2) has to disappear. If each of the terms of the sum vanishes in the following way,

$$\Gamma_{\mathbf{n}'\to\mathbf{n}}P(\mathbf{n}', t) - \Gamma_{\mathbf{n}\to\mathbf{n}'}P(\mathbf{n}, t) = 0, \tag{2.3}$$

then the underlying Markov process fulfills the detailed balance condition, otherwise it is named global balance. Detailed balance is a direct consequence of the microreversibility. The corresponding Markov chain is thus called reversible. It turns out that a system satisfying the condition of detailed balance is in equilibrium. In contrast, for systems out of equilibrium detailed balance is violated. From this point of view, condition (2.3) provides a test to distinguish equilibrium and non-equilibrium states.

Many problems in physics and other sciences can be reduced to the form of a master equation. For example, one can describe chemical processes or population dynamics. Moreover, Eq. (2.2) yields the theory for several NMR experiments explaining nuclear spin relaxation. Furthermore, stochastic particle hopping on a lattice can be reflected by the master equation. These systems, called driven lattice gases, play the role of a paradigm in non-equilibrium statistical mechanics.

2.2 The simple exclusion process

2.2.1 Definition of the model

Driven lattice gases are statistical models based on the Ising concept. They are denoted by particles hopping on a lattice and interacting through hard-core repulsion. Katz, Lebowitz and Spohn defined a general driven lattice gas in their work about fast ionic conductors [KLS84]. Even well before, the simple exclusion process, as a special case of driven lattice gas models, was applied by MacDonald and Gibbs to describe protein synthesis on RNA [MG69]. Independently from them, the Austrian physicist Frank Spitzer used the simple exclusion process to understand interactions of Markov processes [Spi70].

In order to define the simple exclusion process, one considers a one-dimensional lattice, where a microstate of the lattice system is given by $\mathbf{n} = \{n_i\}$, with $n_i = 0$ or 1 depending on whether site i is vacant or occupied by one particle. Thus, occupation numbers satisfy $n_i^k = n_i$ for any integer number k. The hopping dynamics of this lattice gas is controlled by a Poisson process. If Γ is the number of jumps per particle and time unit, the probability $P(t)dt$ of waiting time t between two successive hopping events is given by

$$P(t)dt = \lim_{\Delta t \to 0} \Gamma(1 - \Gamma\Delta t)^{\frac{t}{\Delta t}}\, \Delta t = \Gamma\, \mathrm{e}^{-\Gamma t}\, dt. \tag{2.4}$$

The waiting times are exponentially distributed, as can be seen from (2.4). In other words, every particle has got a clock that rings according to a Poisson process and induces the particle to move. Due to hard-core repulsion, the particle migration is restricted to vacant nearest-neighbor sites. Consequently, the particle on the ith site in Fig. 2.1 may only jump from i to $i+1$ when the clock rings at a time depending on hopping rate $\Gamma_{i \to i+1}$. After the interchange of occupation numbers of sites i and $i+1$, the clock of the affected particle needs to be reset.

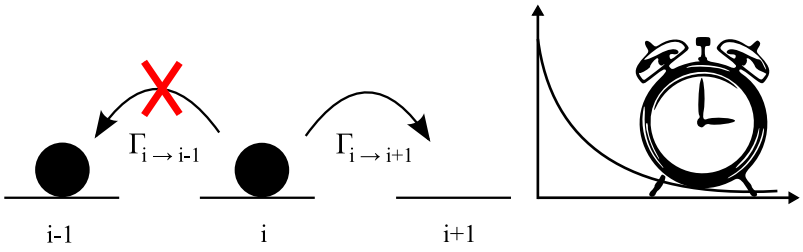

Figure 2.1: Dynamics of the simple exclusion process. The hopping process is defined by transition rates $\Gamma_{i\to i-1}$ and $\Gamma_{i\to i+1}$. The possible jump from i to $i+1$ is performed not before the clock rings.

The hopping rates controlling the particle dynamics allow a classification of the simple exclusion process into three cases. Identical hopping rates in each direction define the symmetric simple exclusion process (SSEP). SSEP is adapted for constructing equilibrium systems. However, when such a system is in contact with particle reservoirs at the left and right boundary of the lattice, this leads to a boundary-driven system with a non-equilibrium steady state. The so-called asymmetric simple exclusion process (ASEP) results from different hopping rates in each direction. In this way, an elementary example for a bulk-driven system is found by using periodic boundary conditions, so that particles move on a ring controlled by the ASEP dynamics. If the hopping rate in one direction is set to zero, hopping events are only observed in the remaining direction. This unidirectional hopping is named totally asymmetric simple exclusion process (TASEP). Despite the simple hopping dynamics, the TASEP offers the same essential features like the more complex ASEP. Hence, the TASEP is much-loved by physicists. The following passage focuses on the integrability of the totally asymmetric simple exclusion process and presents exact results obtained through several approaches.

2.2.2 Integrability of the simple exclusion process

A very simple realization of the TASEP is a ring system with N sites and M particles that only jump in one direction with hopping rate $\Gamma_{i\to i+1} = 1$. Due to periodic boundary conditions, the particle number is conserved. It is immediately clear that the count of allowed configurations is given by the binomial coefficient $\binom{N}{M}$. In the steady state, every configuration is equally likely with probability $\binom{N}{M}^{-1}$. Based on this knowledge, an expression for the steady-state current j, that counts all particles crossing a bond during a time unit, is straightforward to find. According to the TASEP rules, for a successful hopping both an occupied site and a subsequent vacant site are required. This restricts the configuration range and j reads $j = \binom{N}{M}^{-1}\binom{N-2}{M-1} = \frac{M}{N}\frac{N-M}{N-1}$. Applying the thermodynamic limit by making N and M close to infinity at a constant ratio $\frac{M}{N} = \rho$, the current as a function of the particle

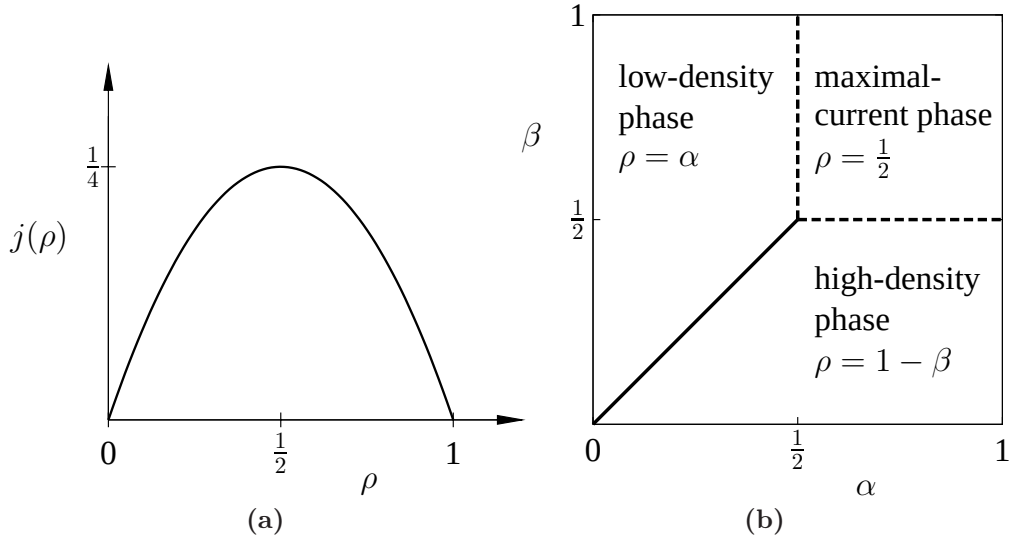

Figure 2.2: Solutions of the TASEP. (a) The bulk current parabola $j(\rho)$ can be obtained by using simple combinatorics. (b) The mean-field phase diagram contains three phases which are parameterized by injection rate α and extraction rate β: maximal-current phase ($\rho = \frac{1}{2}$, $j = \frac{1}{4}$), low-density phase ($\rho = \alpha$, $j = \alpha(1-\alpha)$), high-density phase ($\rho = 1 - \beta$, $j = \beta(1-\beta)$). The solid line denotes a first-order phase transition, whereas dashed lines mark second-order phase transitions.

density ρ is given by a parabola

$$j = \rho(1 - \rho), \tag{2.5}$$

shown in Fig. 2.2a.

For the TASEP with open boundary conditions, it is a nontrivial task to get the exact density profile depending on injection rate α and extraction rate β. Admittedly, mean-field approaches yield the correct phase diagram, as can be seen in Fig. 2.2b, but an exact density calculation along the lattice fails to be achieved. Exact density profiles and further statistical quantities like density correlation functions have been obtained for any N, α and β by recursion formulas [DDM92, SD93]. Two further approaches are known in the driven lattice gas community for solving the (T)ASEP in an exact manner, called matrix approach and Bethe ansatz.

The matrix approach, inspired from the quantum inverse scattering method, was initially used by Derrida et al. to solve the (T)ASEP with open boundary conditions [DEHP93]. According to Derrida, the probability $P(\mathbf{n})$ of a configuration $\mathbf{n} = \{n_1, \ldots, n_N\}$ in the steady state is given as a product of matrices as follows,

$$P(\mathbf{n}) = Z^{-1} \langle W | \prod_{i=1}^{N} [n_i D + (1 - n_i) E] \, | V \rangle \, . \tag{2.6}$$

Z is the normalization factor and reads

$$Z = \sum_{n_1=0,1} \dots \sum_{n_N=0,1} \langle W| \prod_{i=1}^{N} [n_i D + (1-n_i)E] |V\rangle . \tag{2.7}$$

Each site corresponds to a matrix D or E according to the state of the site. Whenever site i is occupied, i.e., $n_i = 1$, matrix D appears in Eqs. (2.6) and (2.7), matrix E is chosen otherwise. A scalar probability is obtained by combining the matrix product with the vectors $\langle W|$ and $|V\rangle$ (bra-ket notation of quantum mechanics). In order to work with Eqs. (2.6) and (2.7), one needs to know some algebraic relations between the matrices D, E and the vectors $\langle W|$, $|V\rangle$. Indeed, they have to satisfy the conditions

$$D|V\rangle = \beta^{-1}|V\rangle \tag{2.8}$$
$$\langle W|E = \alpha^{-1}\langle W| \tag{2.9}$$
$$DE = D + E, \tag{2.10}$$

for the steady state. Nevertheless, it is quite hard to apply this concept, since in general, D and E do not commute. Moreover, these matrices are infinite-dimensional when $\alpha + \beta \neq 1$. A rigorous proof of (2.8)-(2.10) and a pedagogical tutorial for working with this algebra are given by Blythe and Evans [BE07].

The basic idea underlying the exact matrix-product formulation not only allows the well-known mean-field phase diagram to be confirmed (see Fig. 2.2b), but also leads to a more detailed characterization of the single phases. More precisely, the high- and low-density phase decompose into two sub-phases divided by the lines $\alpha = \frac{1}{2}$, $\beta < \frac{1}{2}$ and $\beta = \frac{1}{2}$, $\alpha < \frac{1}{2}$, respectively. These lines separate the parts, where the density profiles approach the bulk value in two different ways. Furthermore, the matrix ansatz deals with exact expressions for all equal-time correlation functions. If a matrix C is defined by $C = D + E$, the averaged site occupation $\langle n_i \rangle$ is

$$\langle n_i \rangle = \sum_{n_1=0,1} \dots \sum_{n_N=0,1} n_i P(\mathbf{n}) = \frac{\langle W| C^{i-1} D C^{N-i} |V\rangle}{\langle W| C^N |V\rangle}. \tag{2.11}$$

Higher correlators emerge as constructions of matrices C, D and E. For example, the two-point correlation function reads

$$\langle n_i n_j \rangle = \sum_{n_1=0,1} \dots \sum_{n_N=0,1} n_i n_j P(\mathbf{n}) = \frac{\langle W| C^{i-1} D C^{j-i-1} D C^{N-j} |V\rangle}{\langle W| C^N |V\rangle}, \tag{2.12}$$

with $i < j$. However, unequal-time correlation functions (for example, $\langle n_i(0) n_j(t) \rangle$) cannot be calculated, not even in the steady state.

Since expressions for computing equal-time correlation functions are available through the matrix approach, a straightforward calculation of the mean current

$j_{i,i+1}$ from i to $i+1$ is possible. Defining $j_{i,i+1}$ by $j_{i,i+1} = \langle n_i(1-n_{i+1})\Gamma_{i\to i+1}\rangle = \langle n_i\rangle - \langle n_i n_{i+1}\rangle$ (for $\Gamma_{i\to i+1}=1$) and using Eqs. (2.11) and (2.12), one has

$$j_{i,i+1} = \frac{\langle W|\, C^{i-1}DEC^{N-i-1}\,|V\rangle}{\langle W|\, C^N\,|V\rangle} = \frac{\langle W|\, C^{N-1}\,|V\rangle}{\langle W|\, C^N\,|V\rangle}. \tag{2.13}$$

As expected in the steady state, Eq. (2.13) is independent from any index denoting the lattice site.

Another approach providing exact solutions of the simple exclusion process is the Bethe ansatz (for review, see [GM06]). It was invented by Bethe to diagonalize the quantum Hamiltonian of the one-dimensional Heisenberg model. Since then, this approach has been extended to other one-dimensional models like the (T)ASEP. For that, the stochastic process of the driven lattice gas has to be translated into the language of a quantum spin Hamiltonian. Especially systems with periodic boundaries can be studied very well by applying the Bethe ansatz [GS92]. But all results obtained by this method are only valid in the steady state. Of course, it is more difficult to calculate exact non-stationary stochastic quantities, since the configuration of a non-stationary system still depends on initial conditions. By using a new form of the Bethe ansatz, the complete master equation at all times was solved for the TASEP on a ring [Pri03].

Inspired by surface growth models, a further approach for solving the (T)ASEP exists. It is possible to map the (T)ASEP on this model class when an occupied site is treated as an elementary downward slope of the surface and an empty site is represented as an upward slope. In this way, a solution for the (T)ASEP is obtained by solving the discrete version of the Kardar-Parisi-Zhang (KPZ) equation. Initially, the KPZ equation describes the evolution of a growing interface profile and turns into the noisy Burgers' equation in the one-dimensional case [KPZ86].

As pointed out here, there are a variety of approaches dealing with exact results for the simple exclusion process. But due to its academic character, the model cannot reflect challenging physical systems without any modifications. Hence, the following section presents the most relevant amendments and extensions of the simple exclusion process.

2.3 Models based on the TASEP

2.3.1 Modelling traffic

Almost every driver knows the feeling of being stuck in a traffic jam. With increasing traffic density, it will be more and more important to understand and predict such congestions on freeways. In order to study traffic flow, some approaches attempt to apply the concept of fluid dynamics, describing the behavior of macroscopic quantities by hydrodynamic formulas. This continuous description, however, exhibits drawbacks concerning the numerical treatment. For example, partial differential equations appear that may lead to numerical instabilities. Furthermore, the hydrodynamic discussion needs a large number of sampling points to get reliable results. All of this amounts to a time-consuming and complicated solution process.

In contrast, discrete approaches do not show these problems and they are therefore of enormous practical relevance. Thus motivated, a discrete model describing vehicle traffic is now presented. It was first proposed by the solid-state physicists Kai Nagel and Michael Schreckenberg to explain the origin of traffic jams [NS92]. According to them, the carriageway is depicted on a one-dimensional array including N sites. Each site is either occupied by a car or empty. Furthermore, cars have an integer velocity between zero and $v_{\max}$. The following four steps are necessary to propagate a car with velocity $v(t)$ at position $x(t)$ in discrete time from t to $t+1$.

1. Acceleration: $v_1(t+1) = \min\left(v(t)+1,\ v_{\max}\right)$
2. Slowing down: $v_2(t+1) = \min\left(v_1(t+1),\ d\right)$
   (d is the distance to the next car at site $x(t)+d+1$.)
3. Randomization: $v_3(t+1) = \begin{cases} \max\left(v_2(t+1)-1,\ 0\right) & \text{with probability } p \\ v_2(t+1) & \text{with probability } 1-p \end{cases}$
4. Car motion: $v(t+1) = v_3(t+1)$
   $x(t+1) = x(t) + v(t+1)$

This algorithm is applied simultaneously (parallel) at time t to each car. After defining the parallel dynamics of the model, the next step is to study the so-called fundamental diagram, which gives a relation between car density and traffic flow. The car density ρ_i on site i and the traffic flow $j_{i,i+1}$ from site i to $i+1$ are measured over a time period T by the following measurement instructions,

$$\rho_i = \lim_{T\to\infty} \frac{1}{T} \sum_{t=t_0+1}^{t_0+T} n_i(t) \tag{2.14}$$

$$j_{i,i+1} = \lim_{T\to\infty} \frac{1}{T} \sum_{t=t_0+1}^{t_0+T} b_{i,i+1}(t), \tag{2.15}$$

where $n_i(t)$ is the occupation number at time t, which is one (zero) if site i is occupied (empty). The motion of a car from i to $i+1$ at time t is indicated by $b_{i,i+1}(t) = 1$. The measurement of quantities begins after the first t_0 time steps. Equations (2.14) and (2.15) demonstrate the simple measurement procedure of macroscopic variables by averaging readily accessible microscopic quantities.

Figure 2.3 displays fundamental diagrams obtained from simulation results. As intuitively expected, the traffic flow is suppressed for increasing p, since p denotes the slowdown probability that characterizes braking behavior and overreaction of drivers. At a critical traffic density, the state of free flow changes to the congested flow part and traffic jams appear. With increasing v and p, this critical value becomes smaller. In Fig. 2.3a, the usual TASEP with parallel update arises using $v_{\max} = 1$ [Hel01], whereas in Fig. 2.3b the particle-hole symmetry is broken by choosing $v_{\max} > 1$. Only for ring systems with particle-hole symmetry ($v_{\max} = 1$), analytical results are available for all probabilities p by using the cluster approximation. This method may be seen as a generalized mean-field theory. In this context, not only one site is considered, but also neighboring sites are involved in the calculation. Following the cluster approximation, j takes the form

$$j = \frac{1}{2}\left(1 - \sqrt{1 - 4(1-p)\rho(1-\rho)}\right). \tag{2.16}$$

Note that for Eq. (2.16) inequality $\langle n_i(1-n_{i+1})\rangle \geq \langle n_i\rangle - \langle n_i\rangle\langle n_{i+1}\rangle$ is satisfied, which implies attraction between particles and holes. This can be verified by comparing (2.16) with the ordinary mean-field current $j = (1-p)\rho(1-\rho)$. Note further that Fig. 2.3a is completely described by Eq. (2.16). On the other hand, deterministic dynamics ($p = 0$) also allows an exact current expression for arbitrary $v_{\max}$. In this case, the current can be written as

$$j = \min\left(v_{\max}\rho,\ 1-\rho\right). \tag{2.17}$$

The linear functions of Eq. (2.17) are plotted in Fig. 2.3 as solid lines.

So far, the applied transition rates have been constant values. But for many physical problems, this simple assumption provides an insufficient description. The following part is devoted to introduce hopping rates as functions of physical quantities and local particle configurations.

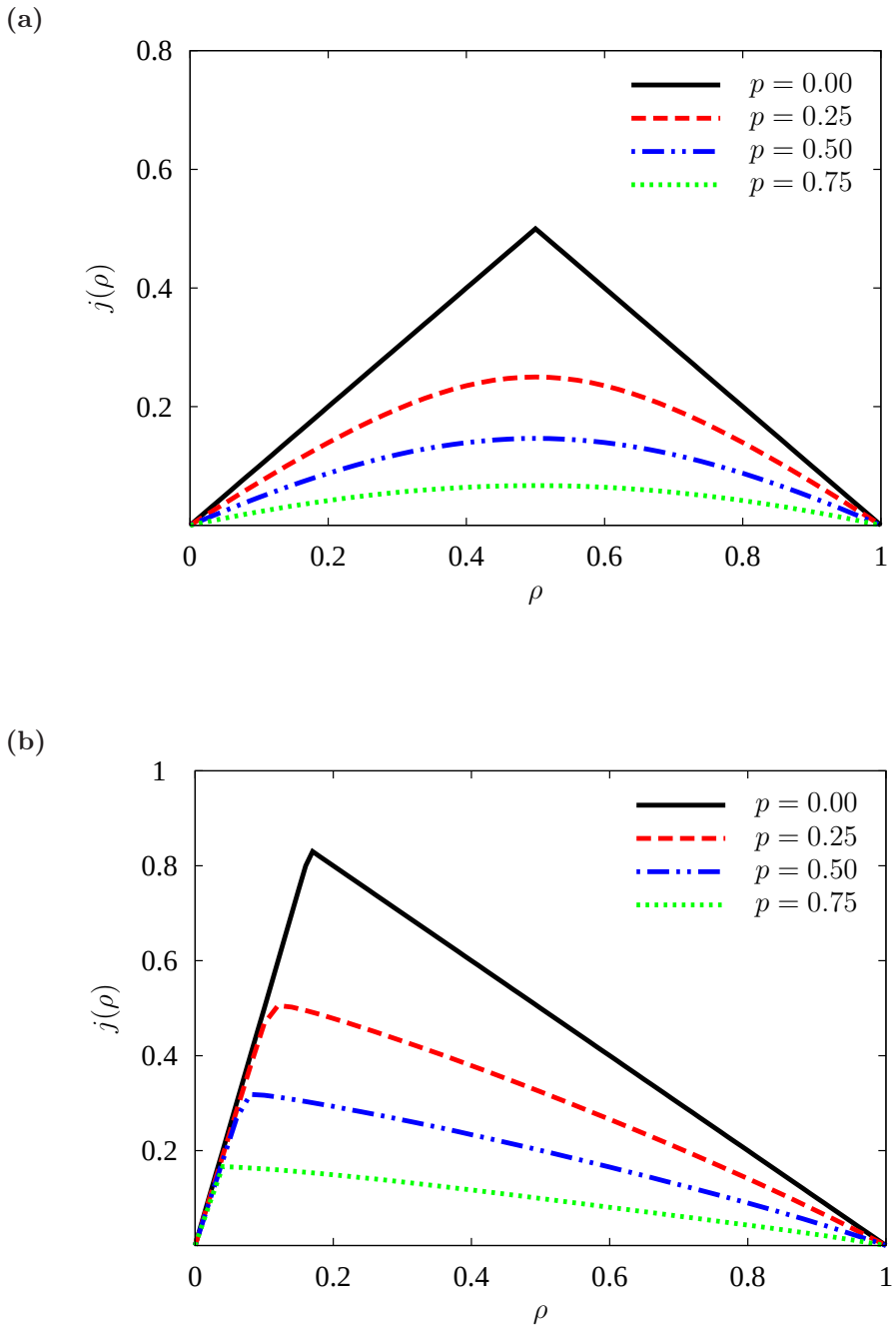

Figure 2.3: Fundamental diagrams. The plots show the traffic flow j versus density ρ with (a) $v_{\max} = 1$ and (b) $v_{\max} = 5$ for several probabilities p reducing the velocity. The curves are from simulating a ring system with $N = 10^4$ and averaging over 10^6 time steps in the steady state.

2.3.2 Modified hopping rates

Physical transport phenomena are in general very complex and arise from an interplay of several particle interactions. Therefore, taking into account additional interactions between particles into the simple exclusion process is a fine step forward. The following paragraph focuses on the TASEP with nearest-neighbor interactions and stochastic update. On the molecular level, important processes in nature can be described by this model [ESDN10].

Let the total energy of the considered system be

$$\mathcal{H}(\mathbf{n}) = \frac{V}{2} \sum_{i \neq j} n_i n_j, \tag{2.18}$$

where V is the interparticle interaction strength. In order to fulfill short-range interactions, the sum only links each site to its nearest neighbors. The dynamics of the system is determined by the hopping rates which result from the existing particle interactions and which are now seen as functions of local particle configurations, i.e., functions of the initial and final state. Using Eq. (2.18), the initial and the final state can be associated with the total energy $\mathcal{H}_i$ and $\mathcal{H}_{i+1}$, respectively. A transition rate consistent to the detailed balance condition is then given by

$$\Gamma_{i \to i+1} = \mathrm{e}^{-\beta(\mathcal{H}_{i+1} - \mathcal{H}_i)/2} \,. \tag{2.19}$$

From now on, the unit of energy is defined by $\beta = 1$.

After insertion of (2.18) into (2.19), the hopping rate can be written in terms of occupation numbers,

$$\begin{aligned} \Gamma_{i \to i+1} &= \mathrm{e}^{-V(n_{i+2} - n_{i-1})/2} \\ &= (1 + n_{i-1}\kappa_+)(1 + n_{i+2}\kappa_-), \end{aligned} \tag{2.20}$$

with $\kappa_\pm = \mathrm{e}^{\pm V/2} - 1$. To be specific, $\Gamma_{i \to i+1}$ takes the following values depending on the local particle configuration:

$$\Gamma_{i \to i+1} = \begin{cases} 1 & \text{for } \circ\ \bullet\ \circ\ \circ \\ \mathrm{e}^{V/2} & \text{for } \bullet\ \bullet\ \circ\ \circ \\ \mathrm{e}^{-V/2} & \text{for } \circ\ \bullet\ \circ\ \bullet \\ 1 & \text{for } \bullet\ \bullet\ \circ\ \bullet \end{cases} \tag{2.21}$$

$$\qquad\qquad\qquad\qquad\quad i{-}1 \quad i \quad i{+}1 \quad i{+}2$$

An empty circle in (2.21) indicates a vacant site and a filled one denotes an occupied site. Since the mean current through a bond $(i,\ i+1)$ is given by $j_{i,i+1} = \langle n_i(1 - n_{i+1})\Gamma_{i \to i+1} \rangle$, together with (2.20) this leads to

$$j_{i,i+1} = \langle n_i(1 - n_{i+1})(1 + n_{i-1}\kappa_+)(1 + n_{i+2}\kappa_-) \rangle \,. \tag{2.22}$$

The current can also be expressed in terms of four-point correlators by expanding Eq. (2.22),

$$\begin{aligned} j_{i,i+1} \;=\; & & \langle (1-n_{i-1})n_i(1-n_{i+1})(1-n_{i+2})\rangle \\ & + \;\; \mathrm{e}^{V/2} & \langle n_{i-1}n_i(1-n_{i+1})(1-n_{i+2})\rangle \\ & + \;\; \mathrm{e}^{-V/2} & \langle (1-n_{i-1})n_i(1-n_{i+1})n_{i+2}\rangle \\ & + & \langle n_{i-1}n_i(1-n_{i+1})n_{i+2}\rangle\,. \end{aligned} \tag{2.23}$$

A numerical discussion of the current is reflected in Fig. 2.4; the stochastic lattice gas with the transition rate (2.21) (Fig. 2.4a) is compared with an equivalent model applying parallel update (Fig. 2.4b) and using transition rate $\min(1, \Gamma_{i\to i+1})$. Both figures show that for large V, the current is strongly suppressed at half filling, see the case $V = 6$. Since the current vanishes for a completely empty or full lattice, a so-called double-hump structure develops in the current-density relation [DFP80, Kru91]. This is an important finding, because the number of extreme values hints to a complex phase transition, as will be shown later.

It is not too surprising that in contrast to the repulsive system, attractive particle interactions do not lead to a second maximum in the current function and no rich phase behavior is thus expected. For $V = -6$ and stochastic update, the current is merely reduced. Here, particles tend to form clusters, so that particle and hole domains develop. On the other hand, for parallel updating, the attractive case is equal to the non-interacting plot since the particle configuration for a suppressed movement from i to $i+1$ does not arise in the steady state, i.e., $\langle n_{i-1}n_i(1-n_{i+1})(1-n_{i+2})\rangle = 0$.

From a physical point of view, Fig. 2.4a shows the more interesting case, because transfer phenomena in nature (for example, electron transport) rely on hopping processes with stochastic update. Chapter 3 discusses several strategies for studying the stochastic TASEP with repulsive nearest-neighbor interactions ($V > 0$).

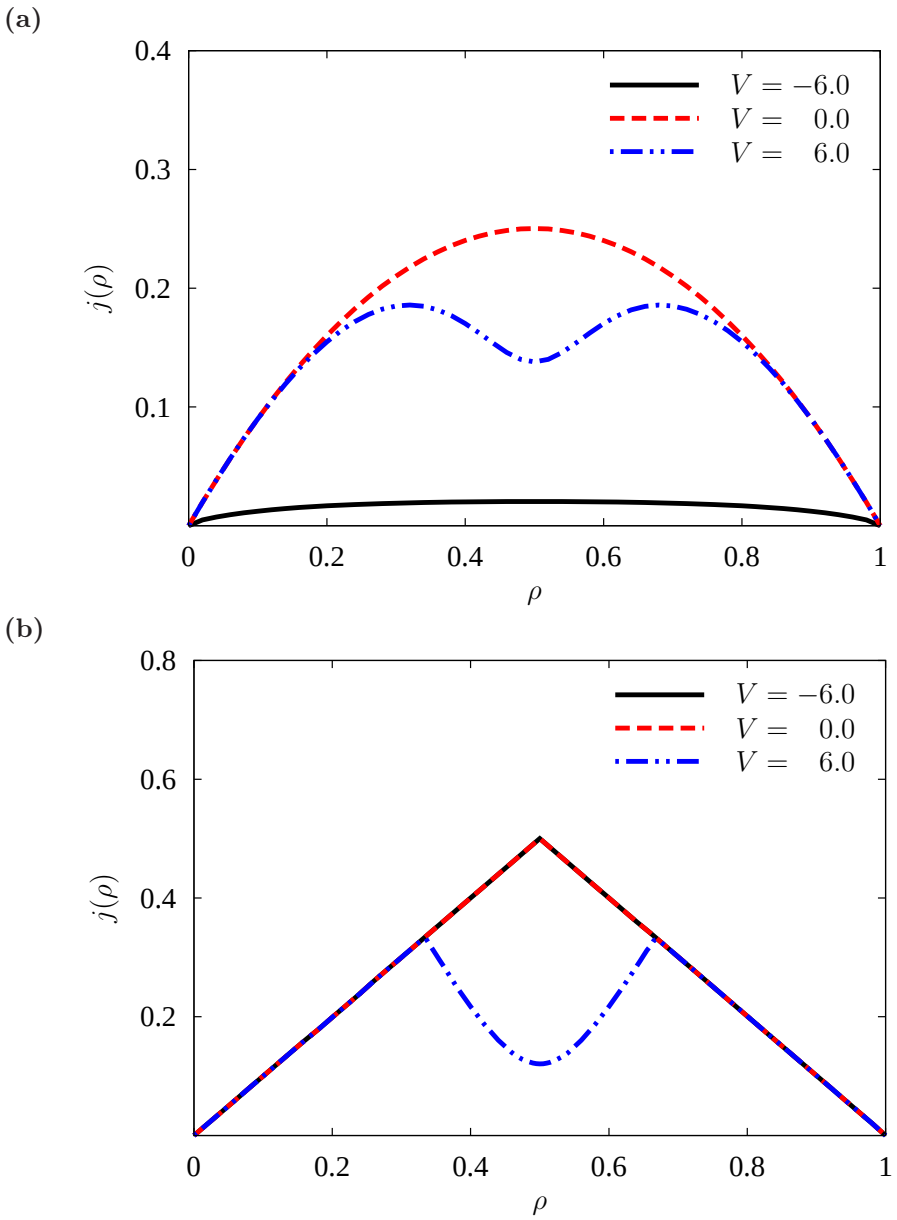

Figure 2.4: Current-density plots for the TASEP with short-range interactions. The graphs are obtained from Monte Carlo simulations using various interaction strengths. The particle dynamics is controlled by rates explained in (2.21), inducing repulsive particle-particle interactions for $V > 0$ and attractive interactions for $V < 0$.
(a) Stochastic update. Monte Carlo simulations are performed on a ring with 10^3 sites. In each case, the current is averaged over a time corresponding to 10^9 jumps in the non-equilibrium steady state.
(b) Parallel update. The current is measured over 10^6 time steps on a ring with 10^3 sites. Note that the probability $\min(1, \Gamma_{i \to i+1})$ is used for particle translocation from i to $i+1$ due to parallel dynamics.

Chapter 3

Studying hopping processes with short-range interactions

This chapter presents various approaches for solving the TASEP with particle-particle interactions. In particular, it discusses analytical techniques like the mean-field approximation and mapping methods based on the usual Ising model. The central part of this chapter is devoted to introduce the classical density functional theory applied to driven lattice gas systems. This local equilibrium theory yields the approximate current and corresponding kinetic equations. The last section is concerned with technical details and settings of Monte Carlo simulations which yield quantitative measures of the quality of expected TDFT data.

3.1 Analytical strategies

This section gives an overview of analytical approaches for one-dimensional driven lattice gases with short-range interactions. One of the simplest approximations is based on the mean-field method, which has become a pedagogic technique for solving the usual TASEP. Therefore, it is interesting to see how far the essential physics of interacting lattice gases is captured in the mean-field current. This investigation also shows whether a qualitatively correct mean-field phase diagram can be expected.

Starting from the master equation describing the dynamics of the system, kinetic equations for all averaged site occupations $\{\rho_i\}\,;\ i = 1, \ldots, N$, can be derived straightforwardly,

$$\frac{d}{dt}\rho_i = j_{i-1,i} - j_{i,i+1}. \tag{3.1}$$

According to Eq. (3.1), the time evolution of the averaged site occupation at the ith site is controlled by an inflow $j_{i-1,i}$ from site $i-1$ to i and a drain $j_{i,i+1}$ through the bond $(i, i+1)$. These currents are in general functions of high-order correlators, even up to four-point correlation functions using current formula (2.23). But one needs a way to calculate these quantities. The mean-field method consists in

replacing such correlators by products of averaged site occupations, for example, $\langle n_i n_j \rangle \approx \langle n_i \rangle \langle n_j \rangle = \rho_i \rho_j$. Thus, all fluctuations are neglected.

In order to proceed, it is worthwhile to find a continuum description of (3.1). For this purpose, a variable $x = ia$ is introduced, so that $0 \leq x \leq 1$. The lattice constant a is defined by the inverse system size, i.e., a approaches zero for large lattices. The density on site $i \pm k$ can thus be written as $\rho_{i\pm k} = \rho(x \pm ka)$, where an expression for $\rho(x \pm ka)$ is found by a Taylor expansion as follows,

$$\rho(x \pm ka) = \rho(x) \pm ka \frac{\partial}{\partial x} \rho(x) + \mathcal{O}(a^2). \tag{3.2}$$

The continuum form of kinetic equation (3.1) is

$$\frac{\partial}{\partial t} \rho + a \frac{\partial}{\partial x} \rho \frac{d}{d\rho} j = 0, \tag{3.3}$$

which reminds of the well-known continuity equation. Inserting the current equation from (2.23) into (3.1) and applying the just explained mean-field technique in combination with the continuum approximation (3.2), a comparison with Eq. (3.3) finally yields the bulk current

$$j(\rho) = \rho + (\Sigma_\kappa - 1)\rho^2 - 2\Sigma_\kappa \rho^3 + \Sigma_\kappa \rho^4, \tag{3.4}$$

with $\Sigma_\kappa = \kappa_- + \kappa_+$. Quadratic and higher-order terms in a were neglected during this procedure. The derived mean-field expression (3.4) is a disappointing result, because a curve sketching does not reveal the two required maxima. Instead, it shows an increased current value at half-filling for a large V. In contrast to the non-interacting ($V = 0$) TASEP or systems with long-range interactions, the mean-field approximation is thus not suitable for driven lattice gas systems with short-range interactions (cf. Appendix A).

However, Katz, Lebowitz and Spohn introduced a technique to treat a particular class of one-dimensional lattice gas models with short-range interactions [KLS84]. According to them, all steady-state quantities can be computed exactly from the equilibrium distribution of the Ising model if it is possible to make the steady state independent from the present bias. To this end, jump rates

$$\Gamma_{i\to i+1}(n_{i-1} = 0, n_i = 1, n_{i+1} = 0, n_{i+2} = 0) = \Gamma^{(1)}_{i\to i+1} \tag{3.5}$$

$$\Gamma_{i\to i+1}(n_{i-1} = 1, n_i = 1, n_{i+1} = 0, n_{i+2} = 0) = \Gamma^{(2)}_{i\to i+1} \tag{3.6}$$

$$\Gamma_{i\to i+1}(n_{i-1} = 0, n_i = 1, n_{i+1} = 0, n_{i+2} = 1) = \Gamma^{(3)}_{i\to i+1} \tag{3.7}$$

$$\Gamma_{i\to i+1}(n_{i-1} = 1, n_i = 1, n_{i+1} = 0, n_{i+2} = 1) = \Gamma^{(4)}_{i\to i+1} \tag{3.8}$$

have to fulfill the relations

$$\Gamma^{(3)}_{i\to i+1} = \mathrm{e}^{-V} \Gamma^{(2)}_{i\to i+1} \tag{3.9}$$

$$\Gamma^{(4)}_{i\to i+1} - \Gamma^{(3)}_{i\to i+1} - \Gamma^{(2)}_{i\to i+1} + \Gamma^{(1)}_{i\to i+1} = 0, \tag{3.10}$$

where $V > 0$ represents repulsive interactions between particles. The configurations in (3.5)-(3.8) denote the occupations of the initial state, i.e., configurations shortly before the jump. However, one-dimensional lattice gases with transition rates (2.21) are not designed to be exactly solvable. To be specific, these rates satisfy condition (3.9), but they do not fulfill relation (3.10).

By contrast, Hager et al. choose rates fulfilling conditions (3.9) and (3.10), so that the equilibrium calculation yields exact results, even though they use a non-equilibrium system [HKPS01]. They fall back on the transfer-matrix technique to compute the TASEP with nearest-neighbor interactions. This method is a powerful technique for solving problems in equilibrium statistical physics (for a detailed discussion, see Appendix B). But results are only valid in the thermodynamic limit. Hence, systems of finite size are not captured. Furthermore, the transfer-matrix method does not care for lattice indices. Consequently, Hager et al. fail to calculate the time evolution of open systems, but only the mean current is available by imposing periodic boundary conditions.

In the run-up to their calculations, they mapped the TASEP onto the Ising spin model. For a better understanding of this concept, consider the Hamiltonian describing the total energy of a one-dimensional Ising system for N spins with nearest-neighbor interactions,

$$\mathcal{H}(\mathbf{s}) = V \sum_{i=1}^{N} s_i s_{i+1} + h \sum_{i=1}^{N} s_i, \tag{3.11}$$

where $s_i = \{-1, 1\}$ is the ith spin and h acts as an external field. Here, periodic boundaries, $s_{N+1} = s_1$, are assumed. The spin Hamiltonian can be reinterpreted as a lattice gas Hamiltonian using the relation $s_i = 1 - 2n_i$ between spin and occupation number. Thus, (3.11) takes the form

$$\mathcal{H}(\mathbf{n}) = V \sum_{i=1}^{N} (1 - 2n_i)(1 - 2n_{i+1}) + h \sum_{i=1}^{N} (1 - 2n_i). \tag{3.12}$$

As can be seen from (3.12), the energy is increased by $4V$ for each occupied neighboring pair.

After testing the quality of approximations widely used for interacting lattice gases, Section 3.2 introduces a technique which will turn out to be an improvement to the presented methods in many respects. Based on the ideas of classical density functional theory and the local equilibrium approximation, this approach solves driven lattice gases with repulsive nearest-neighbor interactions by calculating correlation functions at every order.

3.2 The concept of density functional theory for atomic hopping

3.2.1 Derivation of the current equation

The density functional theory (DFT) applied to classical systems is an excellent method to calculate currents, to derive kinetic equations or to study phase transitions. Initially, it was formulated for continuous fluid systems (for review, see [Löw94]). In [NDM93], the continuous theory was adapted to discrete lattice gases. In this way, the current and all other macroscopic quantities appearing in the lattice system are expected to be functions only of occupation probabilities.

Since the current in Eq. (2.23) exhibits up to four-point correlation functions using transition rate (2.21), it is still an open question to compute the current explicitly, even in the non-equilibrium steady state. Here, a method is described for calculating higher-order correlation functions by utilizing the framework of DFT. The first step is to apply the local equilibrium approximation which means that all non-equilibrium correlators are replaced by corresponding equilibrium quantities with average $\langle \cdots \rangle_{\mathrm{eq}}$. Secondly, the current is completely expressed as a function of occupation probabilities.

Following this outlined procedure, the local equilibrium approximation is applied to the current $j_{i,i+1}$ which formally leads to

$$j_{i,i+1} \simeq \langle n_i(1-n_{i+1})\Gamma_{i\to i+1}\rangle_{\mathrm{eq}}\,. \tag{3.13}$$

For the second step, the equilibrium joint probability

$$P_{\mathrm{eq}}(n_i,\,\ldots,n_{i+j}) = \widetilde{\Gamma}(n_{i+1}|n_i)\prod_{s=2}^{j}\Gamma(n_{i+s}|n_{i+s-1}) \tag{3.14}$$

is introduced. $\Gamma(n_{i+s}|n_{i+s-1})$ denotes the conditional probability of n_{i+s} assuming that n_{i+s-1} has occurred and $\widetilde{\Gamma}(n_{i+1}|n_i)$ is determined by $\Gamma(n_{i+1}|n_i)$ multiplied by the probability of n_i. It is important to realize that the conditional probabilities fulfill the Markov property due to the applied short-range interactions [Bus99]. Linking the joint probability in (3.14) to the corresponding correlator, for example, $P_{\mathrm{eq}}(n_i=1,\,\ldots,n_{i+j}=0)_{\mathrm{eq}} = \langle n_i\ldots(1-n_{i+j})\rangle_{\mathrm{eq}}$ and applying this to Eq. (2.23), the steady-state current is then given by

$$j_{i,i+1} \simeq \sum_{k=0,\,1}\Big[\widetilde{\Gamma}(n_i|1-k) + \xi_k\widetilde{\Gamma}(n_i|k)\Big]\,\Gamma(n_{i+1}|n_i)\,\Gamma(1-k|n_{i+1}), \tag{3.15}$$

with $\xi_k = \mathrm{e}^{(-1)^{k+1}V/2}$, $V \geq 0$ (repulsive interactions) and $n_i = 1 - n_{i+1} = 1$. Equation (3.15) can be understood if one expands this expression and dedicates the resulting terms with four-point correlation functions. A remarkable feature of Eq. (3.15) is

that the conditional probabilities therein only depend on equilibrium two-point correlation functions and averaged site occupations. For example, $\Gamma(n_{i+1}|n_i)$ is given by

$$\begin{aligned}\Gamma(n_{i+1}|n_i) &= \frac{P_{\mathrm{eq}}(n_i=1,\, n_{i+1}=0)}{P_{\mathrm{eq}}(n_i=1)} \\ &= \frac{\langle n_i(1-n_{i+1})\rangle_{\mathrm{eq}}}{\langle n_i\rangle_{\mathrm{eq}}} \\ &= \frac{\rho_i - C_{i,i+1}}{\rho_i}, \end{aligned} \tag{3.16}$$

where $C_{i,i+1}$ denotes the equilibrium pair correlator concerning the sites i and $i+1$. Generalizing Eq. (3.16) for arbitrary sites j and $j+1$ yields

$$\begin{aligned}\Gamma(n_{j+1}|n_j) &= \left(\tfrac{C_{j,j+1}}{\rho_j}\right)^{n_j n_{j+1}} \left(\tfrac{\rho_{j+1}-C_{j,j+1}}{1-\rho_j}\right)^{(1-n_j)n_{j+1}} \\ &\times \left(\tfrac{\rho_j - C_{j,j+1}}{\rho_j}\right)^{n_j(1-n_{j+1})} \left(\tfrac{1-\rho_j-\rho_{j+1}+C_{j,j+1}}{1-\rho_j}\right)^{(1-n_j)(1-n_{j+1})}. \end{aligned} \tag{3.17}$$

According to (3.17), the remaining conditional probabilities in (3.15) are

$$\widetilde{\Gamma}(n_i|k) = C_{i-1,i}^{k}(\rho_i - C_{i-1,i})^{1-k} \tag{3.18}$$

$$\Gamma(1-k|n_{i+1}) = \left(\frac{\rho_{i+2}-C_{i+1,i+2}}{1-\rho_{i+1}}\right)^{1-k} \left(\frac{1-\rho_{i+1}-\rho_{i+2}+C_{i+1.i+2}}{1-\rho_{i+1}}\right)^{k}. \tag{3.19}$$

Note that $\widetilde{\Gamma}(n_i|1-k)$ is obtained by replacing k with $1-k$ in Eq. (3.18).

Following Appendix C, the equilibrium pair correlators in Eqs. (3.16)-(3.19) can be expressed in terms of densities,

$$C_{i,i+1} = \frac{1}{2K}\left[(\Sigma_{i,i+1}-1)K - 1 + \sqrt{\left[(1-\Sigma_{i,i+1})K+1\right]^2 + 4\Pi_{i,i+1}K}\right], \tag{3.20}$$

with $\Sigma_{i,i+1} = \rho_i + \rho_{i+1}$, $\Pi_{i,i+1} = \rho_i\rho_{i+1}$ and $K = \mathrm{e}^V - 1$. By this, $j_{i,i+1}$ is found as a function of the averaged site occupations $\rho_{i-1}, \ldots, \rho_{i+2}$. Section 4.1 deals with an extensive discussion of the obtained current.

3.2.2 Kinetic equations

The static DFT approach is a time-independent theory that captures stationary quantities. Thus, the current is not available in a time-dependent form and the time evolution of non-equilibrium density profiles cannot be studied.

Following Refs. [RD96] and [FRD+98], for a time-dependent theory, the canonical measure (2.1) is extended as follows,

$$P(\mathbf{n},t) = Z(t)^{-1}\,\mathrm{e}^{-\mathcal{H}(\mathbf{n})+\sum_i h_i(t)n_i}, \tag{3.21}$$

where the normalization factor $Z(t)$ is given by

$$Z(t) = \sum_{\mathbf{n}} \mathrm{e}^{-\mathcal{H}(\mathbf{n})+\sum_i h_i(t)n_i}\,. \tag{3.22}$$

In Eqs. (3.21) and (3.22), $\mathbf{h}(t) = \{h_i(t)\}$ denotes a set of single-particle fields representing deviations from the equilibrium. According to Mermin's theorem [Mer65], the single-particle fields are seen to be unique functions of the mean occupations and generate the instantaneous density profile $\boldsymbol{\rho}(t) = \{\rho_i(t)\}$ consistent to the equilibrium DFT at each time. In other words, all equilibrium relations between correlation functions and single-particle densities are used at each time instant in non-equilibrium processes [HDMF04]. This ensures a crossover to the time-dependent density functional theory (TDFT) for classical systems.

Using the average $\langle\ldots\rangle_t$ with respect to the distribution (3.21) in Eq. (3.1), the TDFT equation of motion for the density profile is derived,

$$\frac{d}{dt}\rho_i(t) = j_{i-1,i}(\boldsymbol{\rho}(t)) - j_{i,i+1}(\boldsymbol{\rho}(t)), \tag{3.23}$$

with $j_{i,i+1}(\boldsymbol{\rho}(t)) = \langle n_i(1-n_{i+1})\Gamma_{i\to i+1}\rangle_t$. Inserting current formula (3.15) into (3.23) and applying Eqs. (3.16)-(3.20), all expressions in (3.23) are purely density-dependent. According to Eq. (3.23), these densities are seen to be functions of time. In this way, it is arrived at a closed set of nonlinear differential equations for the time evolution of occupation probabilities. The kinetic equations are solved numerically in Section 4.3 for given boundary conditions (for details, see Section 4.2) and an initial lattice occupation.

3.3 Verifying analytical results

Before further discussing the TDFT results, it is illuminating to prove them numerically by kinetic Monte Carlo (KMC) simulations. The KMC method is a continuous-time Monte Carlo computer simulation intended to simulate the dynamical evolution of processes in real time. Typically, these are processes that occur with given transition rates. Note that the rates are inputs to the KMC algorithm, the method cannot predict them. The KMC procedure [BKL75] is essentially the same as the first reaction method (FRM) developed by Gillespie [Gil76]. The only difference between both algorithms seems to be in the usage areas. KMC is mostly known in physics, while the FRM is mainly applied in chemistry.

The key property of KMC is that events (for example, particle hopping on a lattice) associated with the rates are of the Poisson process type. According to the Poisson process reflected in Eq. (2.4), the hopping time t at which a particle moves from initial site i to final site f is given by

$$t = t_{\text{global}} - \frac{1}{\Gamma_{i\to f}} \ln(1-\sigma)\,, \tag{3.24}$$

where t_{global} denotes the global time, σ is created by a random number generator[1] that yields uniformly distributed values on the interval $[0,\, 1[$ and $\Gamma_{i\to f}$ labels the transition rate.

Before starting the KMC simulation, an initial lattice configuration is required. At the beginning, the tentative times for all possible candidates for a successful move are calculated by use of (3.24) and stored in the so-called event list. If k possible hopping processes are determined, the jump that belongs to the time $t_{\min} = \min(t_1,\, t_2, \ldots,\, t_{k-1},\, t_k)$ is performed. After the selection and the translocation of the particle whose time is minimal, the global time is advanced to the minimum time. Also the event list has to be recalculated, since the particle movement could influence the jump conditions of other particles. In other words, it may be true that several jumps are not possible anymore, new particle movements emerge or certain jumps get new energy environments. After updating the list, the Monte Carlo simulation starts again by searching the event with minimum time. Appendix D gives a detailed description of KMC.

Numerical simulations, such as KMC experiments, necessarily deal with systems of finite size. This causes finite size effects. An easy measure for finite lattice size effects is provided by considering the current in non-interacting ($V = 0$) TASEP systems. Chapter 2 already dealt with the current formula for a ring system with N sites and M particles moving unidirectionally on the lattice. Accordingly, the current reads $j = \frac{M}{N}(1-\frac{M}{N})\frac{N}{N-1}$, where $\frac{M}{N}$ represents the density on the ring. A comparison with the current density relation for $N \to \infty$ defined by Eq. (2.5) yields the finite size factor $\frac{N}{N-1}$. This result obviously leads to higher currents for decreasing

[1] In this thesis, the Mersenne Twister random number generator is used [MN98].

systems sizes. To ensure reliable numerical data in the following evaluations, finite size effects are reduced by using lattices with 10^3 sites for both simulations on a ring and numerical experiments for open systems.

Finally, the difference is pointed out between discrete-time and continuous-time Monte Carlo algorithms concerning the measurement of physical quantities. In contrast to procedures in which time is a discrete value as in the Nagel-Schreckenberg model, continuous-time Monte Carlo algorithms use measurement rules for densities and equal-time correlation functions in an integral form. For instance, Eq. (2.14) has to be rewritten as

$$\rho_i = \lim_{T\to\infty} \frac{1}{T} \int_{t_0}^{t_0+T} dt\, n_i(t), \tag{3.25}$$

where ρ_i is averaged over a time period T. Any higher-order correlation function can be measured in the same way as in (3.25). One should note that Eq. (2.15) for measuring the current still remains unchanged in KMC experiments. In the following chapter, all quantities are observed over a time period that corresponds to 10^9 jumps in the non-equilibrium steady state for getting values averaged reliably. The collection of data begins at time t_0 defined by 10^8 particle movements.

Chapter 4

Results of classical DFT calculations

This chapter begins with discussing the bulk current derived in Section 3.2. In this context, periodic boundary conditions are used. The next section presents techniques to realize open boundary conditions. This is necessary for calculating density profiles. Corresponding time-dependent and steady-state profiles are shown in the last part of this chapter, which is concluded by the steady-state phase diagram. All predictions of the DFT approach are verified by Monte Carlo simulations.

4.1 Discussion of the bulk current

Having derived an analytical expression for the current in the last chapter, the first goal here is to study the current-density relation. For that, a system with periodic boundary conditions is considered. Consequently, none of the statistical quantities of interest show any spatial inhomogeneities in the steady state. Hence, one sets $j_{i,i+1} = j$ in Eq. (3.15) and suppresses all indices in Eq. (3.20).

For V sufficiently close to zero, the equilibrium pair correlator $C(\rho)$ factorizes as follows,

$$\lim_{V\to 0} C(\rho) = \rho^2. \tag{4.1}$$

The validity of (4.1) can easily be comprehended by using correlator equation (C.11) in Appendix C, neglecting all indices there and applying $V = 0$. The simple quadratic form of (4.1) leads to a current approaching the usual TASEP parabola for particles feeling only hard-core repulsion,

$$\lim_{V\to 0} j(\rho) = \rho - \rho^2. \tag{4.2}$$

For increasing V, the current-density relation $j(\rho)$ develops the required double-hump structure with two maxima at densities ρ_1^* and ρ_2^*, when V exceeds a critical value $V_c = -2\ln\left(\sqrt{5}-2\right)$, which is the real solution of

$$\left.\frac{d^2 j(\rho)}{d\rho^2}\right|_{\rho=0.5} = 0. \tag{4.3}$$

Equation (4.3) describes the transition from a maximum to a minimum in $j(\rho)$ at $\rho = 0.5$. In the limiting case $V \to \infty$, the pair correlation function and the current can be written as

$$\lim_{V\to\infty} C(\rho) = \frac{\sqrt{x}-1}{2} + \rho \tag{4.4}$$

$$\lim_{V\to\infty} j(\rho) = \frac{x^{\frac{3}{2}} - 2x + x^{\frac{1}{2}}}{1-x}, \tag{4.5}$$

with $x = (2\rho - 1)^2$. According to (4.5), the particle movement is frozen for a half-filled system and reaches its maxima at $\rho^*_{1,2} = \frac{1}{2} \pm \left(\sqrt{2} - 1\right)/2$ which is in agreement with [Kru91].

A comparison between the analytical findings and KMC simulations is displayed in Figs. 4.1 and 4.2. The pair correlation function $C(\rho)$ and the current-density relation $j(\rho)$ are plotted for different interaction strengths $V = 0$, $V = V_c$, $V = 2V_c$ and $V \to \infty$ in Figs. 4.1a and 4.2a, respectively.

As shown in Eqs. (4.1) and (4.2), DFT findings for vanishing interparticle interactions are equal to the well-known results of the usual TASEP and thus analytical curves and numerical data collapse, see the case $V = 0$ in Figs. 4.1a and 4.2a. Also the limit $V \to \infty$ in these figures shows that DFT curves calculated from (4.4) and (4.5) become indistinguishable from simulation data.

For small V ($V \lesssim V_c$) as well as for strong particle-particle coupling ($V \gtrsim 4V_c$), there is also an excellent agreement with the simulation data, as seen in Figs. 4.1b and 4.2b. Note that one has to take care of half-filled systems with intermediate interaction strength, where analytical results are expected to be only qualitatively correct.

In order to quantify the deviations between DFT and KMC, it is introduced $|\Delta C(V)|$ and $|\Delta j(V)|$ describing the absolute value of the difference between analytical and numerical results for a given V in a half-filled lattice. These quantities are displayed in the insets of Figs. 4.1b and 4.2b. As discussed above, DFT results perfectly match with KMC data for small V, i.e., $|\Delta C(V)| \approx 0$ and $|\Delta j(V)| \approx 0$. The maximum error of the pair correlator and the current function is located at $2.0\,V_c$ and $2.4\,V_c$, respectively. At these points, the relative error amounts to over $100\,\%$ for both $C(V)$ and $j(V)$. For strong particle-particle coupling, results nicely agree again with numerical solutions, i.e., $|\Delta C(V)|$ and $|\Delta j(V)|$ become small in this regime.

The discussion of $j(\rho)$ is concluded with a surprising result for weak coupling strengths. Analytical predictions and simulations at small V show that low particle-particle interactions induce an increased current compared to the case $V = 0$, see $j(\rho)$ for $V = V_c$ in Fig. 4.2a. To understand the origin of this phenomenon, an analysis of the single correlation functions forming the current has to be performed (cf. Eq. (2.23)). It reveals that each correlator term (correlation function times corresponding transition rate) is larger for small V than its counterpart for $V = 0$.

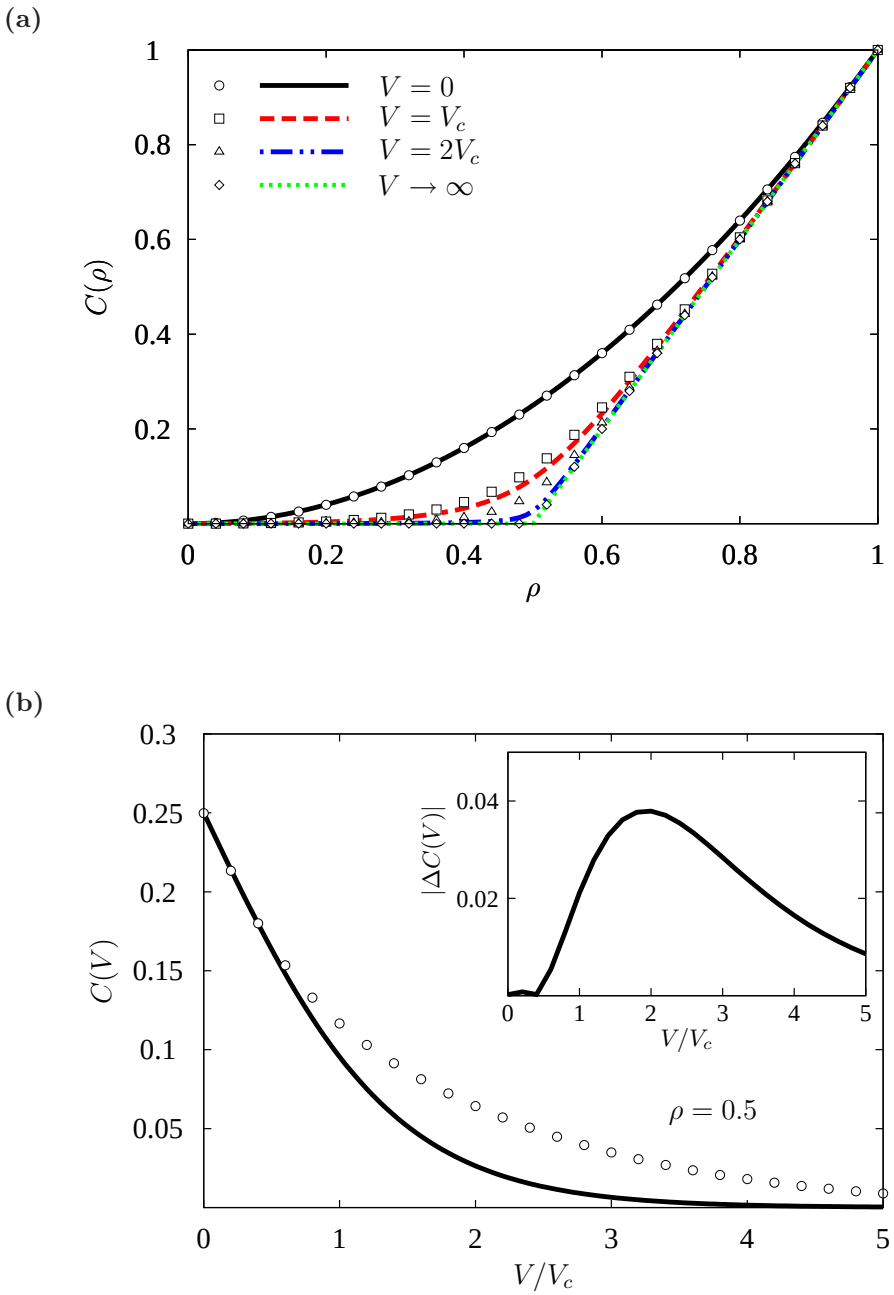

Figure 4.1: (a) Equilibrium pair correlator $C(\rho)$ depending on density ρ for several interaction strengths V calculated by Eq. (3.20) and (b) equilibrium pair correlator $C(V)$ depending on V for fixed density $\rho = 0.5$. Analytical results (lines) are compared by the true non-equilibrium quantities obtained using KMC simulations (symbols) for a ring system with 1000 sites. Each data point is averaged over a time corresponding to 10^9 particle jumps in the steady state. The inset in Fig. 4.1b shows the difference $|\Delta C(V)|$ between analytical and numerical solutions for half-filled systems.

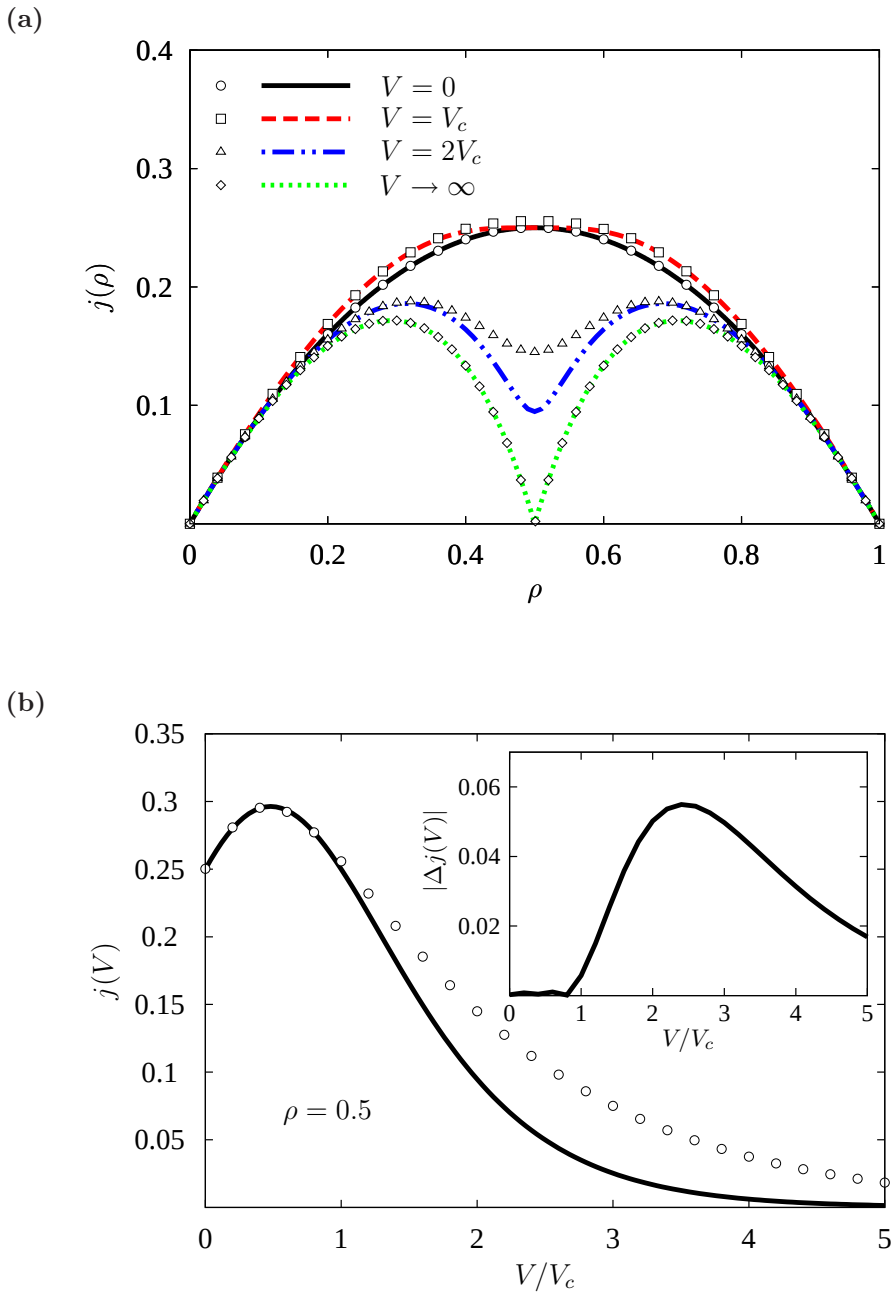

Figure 4.2: (a) Current-density relation $j(\rho)$ for several interaction strengths V calculated by Eq. (3.15) and (b) current $j(V)$ as a function of V for fixed density $\rho = 0.5$. Data points are obtained by KMC simulations with the same system parameters and statistics as in Fig. 4.1. The inset in Fig. 4.2b displays the difference $|\Delta j(V)|$ between analytical and numerical findings for half-filled systems.

This arises partially from transition rates being larger than one and partially from a slightly increased particle-hole attraction.

The use of periodic systems has permitted investigations of the bulk current. By contrast, systems with open boundaries allow studies of density profiles and phase transitions. To this end, two distinct couplings of a lattice system to particle reservoirs are presented in the next section.

4.2 Coupling to boundary reservoirs

4.2.1 Coupling mechanism I

The previous section investigated the bulk behavior of a lattice gas, where the number of particles is conserved within the system. Now this part is focused on the properties of driven lattice gases with open boundaries. In other words, consider a finite system of length N which is coupled at both ends to particle reservoirs with fixed densities. Such models are of enormous relevance for many transport devices, as for molecular wire junctions [NR03, GRN05] or for membrane channels transporting ions [GKCN04]. Basically, two different methods for realising open boundary conditions exist, which differ from each other in the interacting behavior between reservoirs and bulk system. To be specific, there are non-interacting particle baths and reservoirs interacting with the lattice system.

The first coupling mechanism to be presented here is based on the definition of the chemical potential μ [EKMN10, ESDN10]. The chemical potential is a measure of how much the energy of a system changes if a particle is added or removed. On the assumption of fermionic baths in equilibrium, quantum statistics yields the reservoir densities ρ_L and ρ_R for the left and the right boundary, respectively, by use of the Fermi-Dirac distribution

$$\rho_{L,R} = \frac{1}{1 + \mathrm{e}^{-\mu_{L,R}}}, \tag{4.6}$$

where μ_L and μ_R denote the respective chemical potentials of the baths. Here, an injection/extraction mechanism is chosen, where the particles on the lattice do not interact with the particles in the reservoir. The following rates are those that are affected by the coupling mechanism,

$$\begin{aligned} \Gamma_{L\to 1} &= \mathrm{e}^{\mu_L/2} && (4.7)\\ \Gamma_{1\to 2} &= \mathrm{e}^{-\mathcal{H}_2/2} && (4.8)\\ \Gamma_{N-1\to N} &= \mathrm{e}^{\mathcal{H}_{N-1}/2} && (4.9)\\ \Gamma_{N\to R} &= \mathrm{e}^{-\mu_R/2}, && (4.10) \end{aligned}$$

where $\mathcal{H}_2$ ($\mathcal{H}_{N-1}$) is either V or zero, depending on whether site 3 ($N-2$) is occupied or empty. To summarize, hopping into the system is independent from the occupation of the second site, only a first vacant site is required. On the other hand, particle translocation from the first to the second site is not influenced by the reservoir.

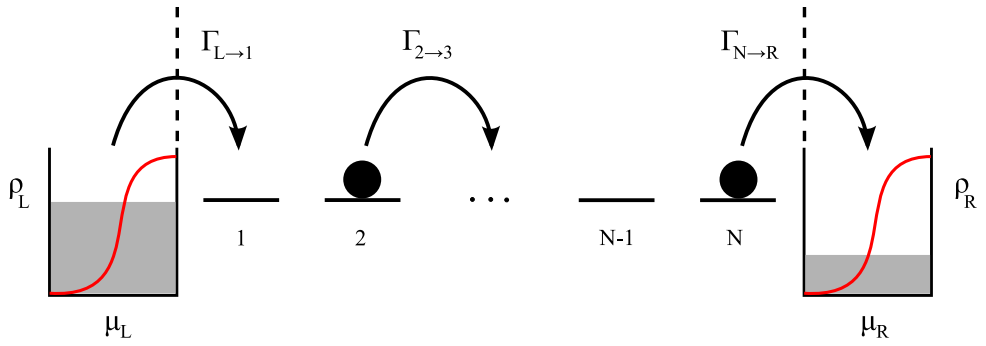

Figure 4.3: Open boundary conditions realized by chemical potentials μ_L and μ_R. On the assumption of a fermionic bath in equilibrium, μ_L and μ_R determine the left and the right reservoir densities ρ_L and ρ_R by considering $\rho_{L,R} = \frac{1}{1+\mathrm{e}^{-\mu_{L,R}}}$ (red graphs in the particle reservoirs). The baths do not interact with the system, denoted by the vertical dashed lines. Rates at the system boundaries (e.g., $\Gamma_{L\to 1}$ and $\Gamma_{N\to R}$) have to take this into account, while bulk rates (e.g., $\Gamma_{2\to 3}$) are defined by Eq. (2.21).

Using similar arguments, one can discuss the rates at the right boundary. Note that in the bulk, the hopping rate (2.21) still remains unchanged. Figure 4.3 is a sketch of the present coupling mechanism.

For an analytical investigation of the open system, equations of all averaged net currents are needed in a first step. Secondly, DFT yields approximate expressions of these currents in terms of densities. To carry through this procedure, one starts with computing the boundary currents. Using rates (4.7) and (4.10), the mean currents transporting particles in the lattice and out of the lattice are

$$j_{L,1} = (\langle n_L\rangle - \langle n_L n_1\rangle)\,\mathrm{e}^{\mu_L/2} \tag{4.11}$$

$$j_{N,R} = (\langle n_N\rangle - \langle n_N n_R\rangle)\,\mathrm{e}^{-\mu_R/2}\,. \tag{4.12}$$

The two-point correlators $\langle n_L n_1\rangle$ and $\langle n_N n_R\rangle$ are easy to calculate by use of the mean-field ansatz, because the system and the baths do not interact. Expressions (4.11) and (4.12) can then be calculated as

$$j_{L,1} = (\rho_L - \rho_L\rho_1)\,\mathrm{e}^{\mu_L/2} \tag{4.13}$$

$$j_{N,R} = (\rho_N - \rho_N\rho_R)\,\mathrm{e}^{-\mu_R/2}\,. \tag{4.14}$$

The currents close to the boundaries, $j_{1,2}$ and $j_{N-1,N}$, are also influenced by the coupling mechanism. These currents consist of three-point correlation functions. Using the DFT approach explained in Section 3.2 and applying rates (4.8) and (4.9), $j_{1,2}$ and $j_{N-1,N}$ read

$$j_{1,2} = \widetilde{\Gamma}(n_2|n_1)\sum_{k=0,1}\Gamma(k|n_2)\zeta_k^- \tag{4.15}$$

$$j_{N-1,N} = \Gamma(n_N|n_{N-1})\sum_{k=0,1}\widetilde{\Gamma}(n_{N-1}|k)\zeta_k^+, \tag{4.16}$$

with $\zeta_k^{\pm} = k\kappa_{\pm} + 1$, $n_1 = n_{N-1} = 1$ and $n_2 = n_N = 0$. By this, three-point correlators are reduced to two-point correlators which can be converted into single-particle densities by Eq. (3.20). The remaining currents in the bulk are given by Eq. (3.15). Having defined the local currents, density profiles can be obtained analytically by solving Eq. (3.23) for each lattice site.

It is clear that the structure of boundary currents (4.13)-(4.16) is different from those of the bulk. Consequently, the boundaries represent inhomogeneities of the system. Thus, resulting profiles in the steady state exhibit non-universal phenomena like density oscillations at the boundaries. This causes effective boundary densities which are determined by the details of the coupling mechanism. These quantities actually control the open system [AS00].

In order to test the results of the kinetic equations numerically, Monte Carlo simulations are performed. In this context, it is a problem to handle the injection and extraction rates since the reservoirs are only defined by chemical potentials. In a given time, one does not know whether the left reservoir, for instance, provides a particle for hopping into the system or not. However, averaged boundary rates can be calculated by taking into account the reservoir densities from (4.6). These rates are given by

$$\langle \Gamma_{L,1} \rangle = \frac{\langle n_L(1-n_1) \rangle}{1-\langle n_1 \rangle} \, \mathrm{e}^{\mu_L/2} = \frac{\rho_L(1-\rho_1)}{1-\rho_1} \, \mathrm{e}^{\mu_L/2} = \rho_L \, \mathrm{e}^{\mu_L/2} \tag{4.17}$$

$$\langle \Gamma_{N,R} \rangle = \frac{\langle n_N(1-n_R) \rangle}{\langle n_N \rangle} \, \mathrm{e}^{-\mu_R/2} = \frac{\rho_N(1-\rho_R)}{\rho_N} \, \mathrm{e}^{-\mu_R/2} = (1-\rho_R) \, \mathrm{e}^{-\mu_R/2}. \tag{4.18}$$

The KMC time for hopping into the system is calculated by inserting (4.17) into (3.24) if the first lattice site is vacant. For a particle at the Nth site, the extraction time is computed in an analogous way by applying rate (4.18). The remaining rates are not influenced by the reservoirs. Consequently, they are determined explicitly in each Monte Carlo step by use of the local particle configuration.

4.2.2 Coupling mechanism II

The aforementioned effective densities are anything but suitable for studying open systems. Since they depend on the precise nature of the coupling mechanism and on the nature of particle interactions between reservoirs and system, resulting density profiles and phase diagrams are also non-universal. For purposes of theoretical investigations, one would like to have a constant density profile along the lattice, where effective boundary densities are identical to the reservoir densities. By this, phase diagrams can be parameterized by ρ_L and ρ_R without thinking about effective densities. In order to obtain a smooth profile, the coupling mechanism has to include particle interactions between reservoir and system in the same way as in the bulk. This assumption provides a homogeneous system concerning the structure of the local currents.

Another advantage of this coupling procedure is the simple realization in TDFT. For systems with short-range interactions, current formula (3.15) is inserted into Eq. (3.23) for each lattice site. This implies some densities which are out of the defined lattice of length N. These densities specify the open system. The left and the right boundary of the lattice are defined by setting $\rho_i(t) = \rho_L$ for $i < 1$ and $\rho_i(t) = \rho_R$ for $i > N$, respectively.

An implementation of this coupling technique in Monte Carlo simulations is not readily possible. As in Section 4.2.1, only the densities of the reservoirs are known, but explicit rates by which particles enter/leave the lattice are not accessible. Again, a possible solution is to specify the injection/extraction dynamics by averaged hopping rates. For example, the averaged injection rate for hopping into the system is

$$\langle \Gamma_{L\to 1} \rangle = \sum_{i,j=0,1} \alpha_{ij} \frac{\langle i10j \rangle_{\rho_L}}{\langle 0j \rangle_{\rho_L}} \delta_{n_2 j}, \tag{4.19}$$

with $\boldsymbol{\alpha} = (\alpha_{ij})_{i=0,1,j=0,1} = \begin{pmatrix} 1 & \mathrm{e}^{-V/2} \\ \mathrm{e}^{V/2} & 1 \end{pmatrix}$.

Because of the hard-core exclusion, (4.19) can only be applied if the first lattice site is empty. However, the injection rate also depends on the occupation of site 2, denoted by the Kronecker delta $\delta_{n_2 j}$. To have a specific example, consider the case $n_1 = 0$ and $n_2 = 0$. $\langle \Gamma_{L\to 1} \rangle$ is then defined to be

$$\langle \Gamma_{L\to 1} \rangle = \frac{\alpha_{00} \langle 0100 \rangle_{\rho_L} + \alpha_{10} \langle 1100 \rangle_{\rho_L}}{\langle 00 \rangle_{\rho_L}} = \frac{\langle 0100 \rangle_{\rho_L} + \mathrm{e}^{V/2} \langle 1100 \rangle_{\rho_L}}{\langle 0000 \rangle_{\rho_L} + \langle 1000 \rangle_{\rho_L} + \langle 0100 \rangle_{\rho_L} + \langle 1100 \rangle_{\rho_L}}, \tag{4.20}$$

where expectation values like $\langle 1100 \rangle_{\rho_L} = \langle n_i n_{i+1} (1 - n_{i+2})(1 - n_{i+3}) \rangle_{\rho_L}$ are stationary-state correlation functions in the thermodynamic limit with particle density ρ_L. α_{00}, α_{10} are entries of matrix $\boldsymbol{\alpha}$ which contains all possible values of (2.21).

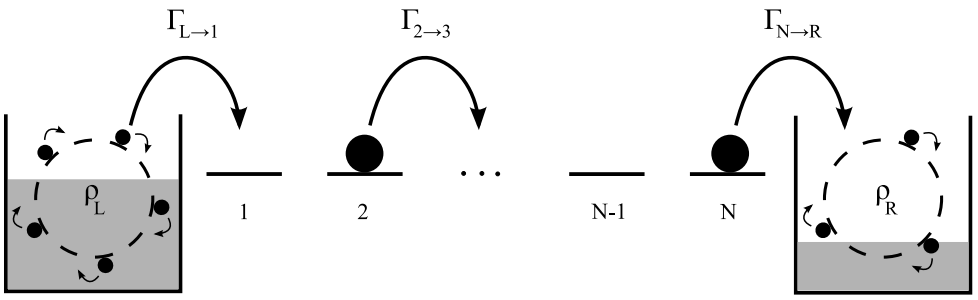

Figure 4.4: Open boundary conditions realized by reservoir densities ρ_L and ρ_R. The particles in the baths interact with particles in the system in the same way as among each other on the lattice. Hence, the injection rate $\Gamma_{L\to 1}$, the extraction rate $\Gamma_{N\to R}$ and bulk rates (e.g., $\Gamma_{2\to 3}$) have the same functional structure. Reservoir details necessary for Monte Carlo simulations are obtained from ring systems with densities ρ_L and ρ_R, respectively.

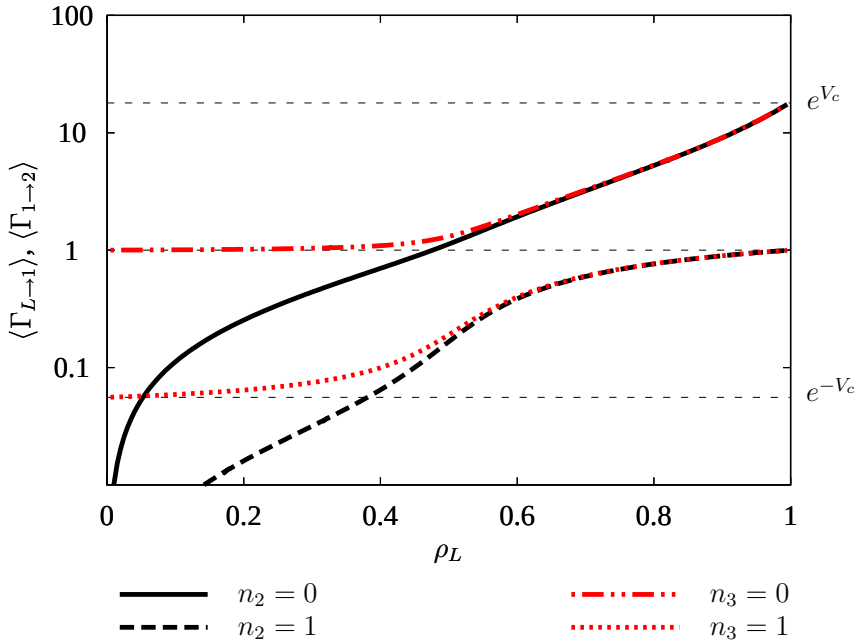

Figure 4.5: Transition rates $\langle\Gamma_{L\to 1}\rangle$ (black) and $\langle\Gamma_{1\to 2}\rangle$ (red) as functions of the reservoir density ρ_L in a semi-log plot. The KMC data come from systems of size $N = 1000$ with $V = 2V_c$.

Analogous to (4.19), the averaged rate for extraction is given by

$$\langle \Gamma_{N\to R} \rangle = \sum_{i,j=0,1} \alpha_{ji} \frac{\langle j10i \rangle_{\rho_R}}{\langle j1 \rangle_{\rho_R}} \delta_{n_{N-1}j}. \tag{4.21}$$

Note that the injection/extraction rates do not completely define the KMC experiments, because particles hopping from 1 to 2 as well as from $N-1$ to N still feel the presence of the reservoirs. These rates are constructed in the same way as shown above,

$$\langle \Gamma_{1\to 2} \rangle = \sum_{i,j=0,1} \alpha_{ij} \frac{\langle i10j \rangle_{\rho_L}}{\langle 10j \rangle_{\rho_L}} \delta_{n_3 j} \tag{4.22}$$

$$\langle \Gamma_{N-1\to N} \rangle = \sum_{i,j=0,1} \alpha_{ji} \frac{\langle j10i \rangle_{\rho_R}}{\langle j10 \rangle_{\rho_R}} \delta_{n_{N-2}j}\,. \tag{4.23}$$

In practice, the two-, three-, and four-point correlators appearing in (4.19)-(4.23) can easily be measured by simulating a large ring system with the same dynamics applied to the open system and using the associated reservoir density $\rho_{L,R}$. This idea is illustrated in Fig. 4.4. Having the required correlation values, Eqs. (4.19)-(4.23) yield the averaged rates for the injection/extraction mechanism. As an example, Fig. 4.5 displays the injection rates $\langle \Gamma_{L\to 1} \rangle$ and $\langle \Gamma_{1\to 2} \rangle$ as functions of the left reservoir density ρ_L, obtained for $N = 1000$ and $V = 2V_c$. This plot shows the influence of the occupation numbers n_2 and n_3 on the rates.

Finally, the distinctions between both coupling techniques, presented in this thesis, are summarized. To this end, consider an open system for each coupling mechanism, corresponding to the boundary conditions $\rho_L = \rho_R = 0.5$. It is evident from Fig. 4.6 that both profiles develop different bulk densities although they result from the same boundary conditions. This fact leads to the conclusion that the coupling mechanism is the most important factor in influencing the behavior of open systems.

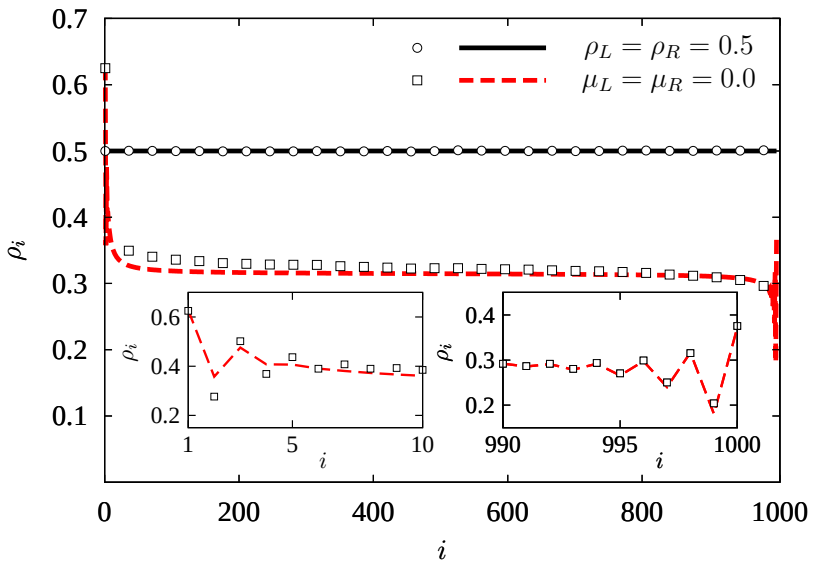

Figure 4.6: Comparison of coupling mechanisms. Although both density profiles arise from the same reservoir densities ($\mu_{L,R} = 0.0$ corresponds to $\rho_{L,R} = 0.5$) and use the same interaction strength $V = 2V_c$, they develop different bulk densities. The coupling technique using chemical potentials exhibits density oscillations at the boundaries (see insets). The second method leads to a smooth profile. The solutions calculated by using TDFT (lines) are verified by KMC simulations (symbols) for a system size of $N = 1000$. For averaging the data points, see Section 3.3.

4.3 Kinetics of density profiles

In order to study density profiles, kinetic equation (3.23) is analyzed. Choosing $V = 0$ allows the access to non-interacting systems, while using the double critical value $2V_c$ enables investigations of lattice gas kinetics with particle-particle interactions. Since the case $V = 2V_c$ has shown unsatisfying results for $j(\rho)$ close to $\rho = 0.5$, as can be seen in Fig. 4.2, this worst-case scenario permits the best evaluation of approximation limits. To have a specific example, consider an initially empty lattice, i.e., $\boldsymbol{\rho}(t = 0) = 0$, with $\rho_L = 0.4$ and $\rho_R = 0.1$. For reasons explained in the previous section, the particle injection/extraction technique is applied, leading to smooth profiles (coupling mechanism II). For the present system, the solutions of Eq. (3.23)[1] at times $t = 500$, 1000, 2000, 4000 and for $t \to \infty$ are compared with corresponding density profiles from KMC simulations. Results are shown in Figs. 4.7a and 4.8a. The Monte Carlo data are seen to be in good agreement with the analytical predictions, see Figs. 4.7b and 4.8b for a quantitative analysis. Obviously, the distinctions between TDFT and KMC findings depend on the curvature of the profiles. Note that the percentages in these plots arise by normalizing the absolute value of $|\Delta\rho_i|$ with

[1]Kinetic equations are solved by the computer algebra system Maple.

regard to the corresponding bulk density. For $V = 0$, the bulk density is determined by the left boundary, i.e., $\rho_B = \rho_L$. In contrast, the case $t \to \infty$, $V = 2V_c$ yields $\rho_B = \rho_1^*$. The latter case defines a phase which does not occur in the usual TASEP. Thus motivated, the density-parameterized phase diagram for $V = 2V_c$ is calculated analytically.

Figure 4.9a shows the resulting steady-state phase diagram. As expected from previous studies of the current-density relation (see Section 4.1), one finds a richer phase behavior for $V = 2V_c$, compared to the well-known one obtained from the ordinary TASEP (cf. Fig. 2.2b). To be specific, there are seven distinct phases instead of three separating through first- and second-order transitions. There arises two maximal-current phases characterized by the bulk densities ρ_1^* and ρ_2^*. Additionally, one notices a region determined by the local minimum in the current-density relation, called minimal-current phase. The remaining four domains are determined by the reservoir densities ρ_L and ρ_R. A low ρ_R effects the so-called low-density phase, whereas a high ρ_R leads to the high-density phase. For each phase, representative density profiles are plotted in Fig. 4.9b. The overall agreement between simulated phase lines or rather KMC density profiles and the TDFT predictions is very good. There are only some evident deviations at the boundaries of the minimal-current phase neighboring the low- and high-density region.

In the process of mapping out the phase diagram, it turns out that TDFT can well account for detecting phase transitions of driven systems. This is illustrated in Fig. 4.10 showing open systems with $V = 2V_c$ and boundary conditions defined in Table 4.1. Figure 4.10a displays a first-order phase transition and in Fig. 4.10b a phase transition of second order is plotted. As seen from these figures, in KMC simulations the finite size effect is of enormous relevance for locating phase transitions of first or second order, since this wipes out the singular behavior occurring in the thermodynamic limit.

It has been shown in previous studies that the shape of the phase diagram can be understood by the current extremal principle [Kru91, OJ98, PS99, HKPS01],

$$j = \begin{cases} \max\limits_{\rho \in [\rho_R, \rho_L]} j(\rho) & \text{for } \rho_L > \rho_R \\ \min\limits_{\rho \in [\rho_L, \rho_R]} j(\rho) & \text{for } \rho_L < \rho_R. \end{cases} \tag{4.24}$$

The first relation (current maximization) is an extension of Krug's maximum-current principle [Kru91] to arbitrary ρ_R [OJ98]. It is applied if the density gradient $\rho_R - \rho_L$ is negative. The second part of (4.24) (current minimization) was first suggested by Popkov and Schütz [PS99]. It states that the system minimizes its current if the density gradient is positive. Note that in general one has to use effective boundary densities in Eq. (4.24) instead of the actual reservoir densities. The special coupling technique (coupling mechanism II), however, allows this notation by making effective and reservoir densities identical. A rigorous proof of the extremal principle is given in [BGRS02].

ρ_L	ρ_R	ρ_B	ρ_L	ρ_R	ρ_B
0.59	0.39	0.39	0.45	0.49	0.49
0.60	0.40	kink	0.45	0.50	0.50
0.61	0.41	0.61	0.45	0.51	0.50

Table 4.1: Open systems for $V > V_c$.

To clarify the extremal principle by specific examples and to provide a test of TDFT, consider again the open systems defined in Table 4.1. The first two columns construct open systems with a negative density gradient, i.e., $\rho_R - \rho_L < 0$. According to Eq. (4.24), the maximum-current principle is applied. Using $\rho_L = 0.59$ and $\rho_R = 0.39$ and making use of $j(\rho)$ corresponding to $V = 2V_c$ (cf. Fig. 4.2a), the largest current value for ρ ranging from ρ_R to ρ_L is found to be $j(\rho_R)$. Consequently, the bulk value is determined by the right boundary density. For $\rho_L = 0.6$ and $\rho_R = 0.4$, one finds two equal maximum values in the current function within the range $[\rho_R, \rho_L]$, namely at ρ_R and ρ_L. This phase is thus called coexisting phase. The third example provides the maximum current at ρ_L leading to a bulk density controlled by the left reservoir. According to this, the system undergoes a first order phase transition which is in agreement with profiles in Fig. 4.10a. Applying the minimal-current relation for the last three open systems given in Table 4.1 (Here, one has $\rho_R - \rho_L > 0$.), the following bulk densities for increasing ρ_R are found: $\rho_B = \rho_R$, $\rho_B = 0.5$, $\rho_B = 0.5$. This is a phase transition of second order, reflected in Fig. 4.10b. Analogously, the deviations between TDFT and KMC phase lines in Fig. 4.9a can be understood by using this concept.

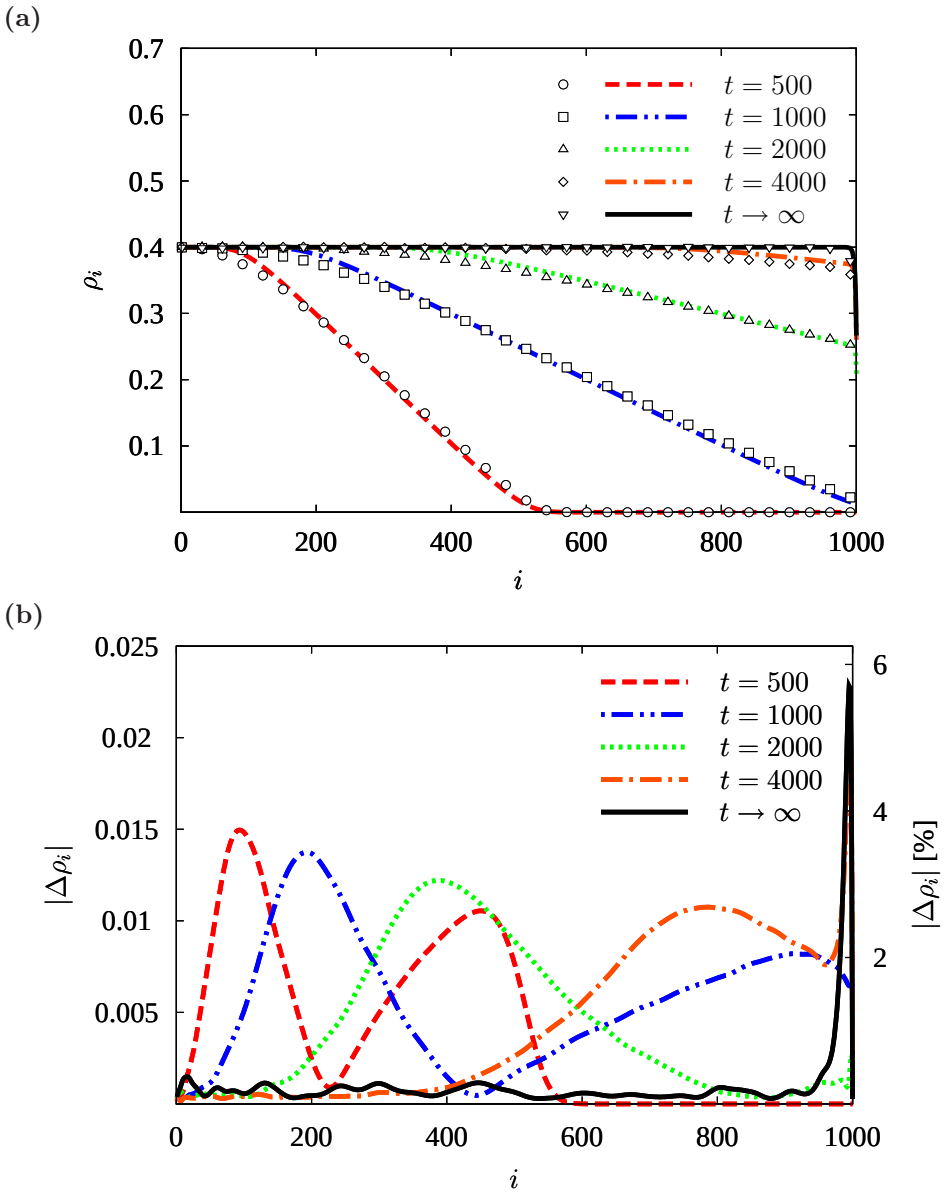

Figure 4.7: (a) Time evolution of a one-dimensional lattice gas corresponding to $\rho_{\mathrm{L}} = 0.4$, $\rho_{\mathrm{R}} = 0.1$, $V = 0$, $N = 1000$. At time $t = 0$, the lattice is empty. Density profiles are shown for $t = 500, 1000, 2000, 4000$ and for the steady state. The solutions calculated using TDFT (lines) are verified by Monte Carlo simulations (symbols), whereby each density profile is averaged over 10^6 configurations. (b) Deviation $|\Delta\rho_i|$ between TDFT and KMC results. It is also shown $|\Delta\rho_i|$ measured relative to the bulk density $\rho_B = \rho_L$ (see right axis).

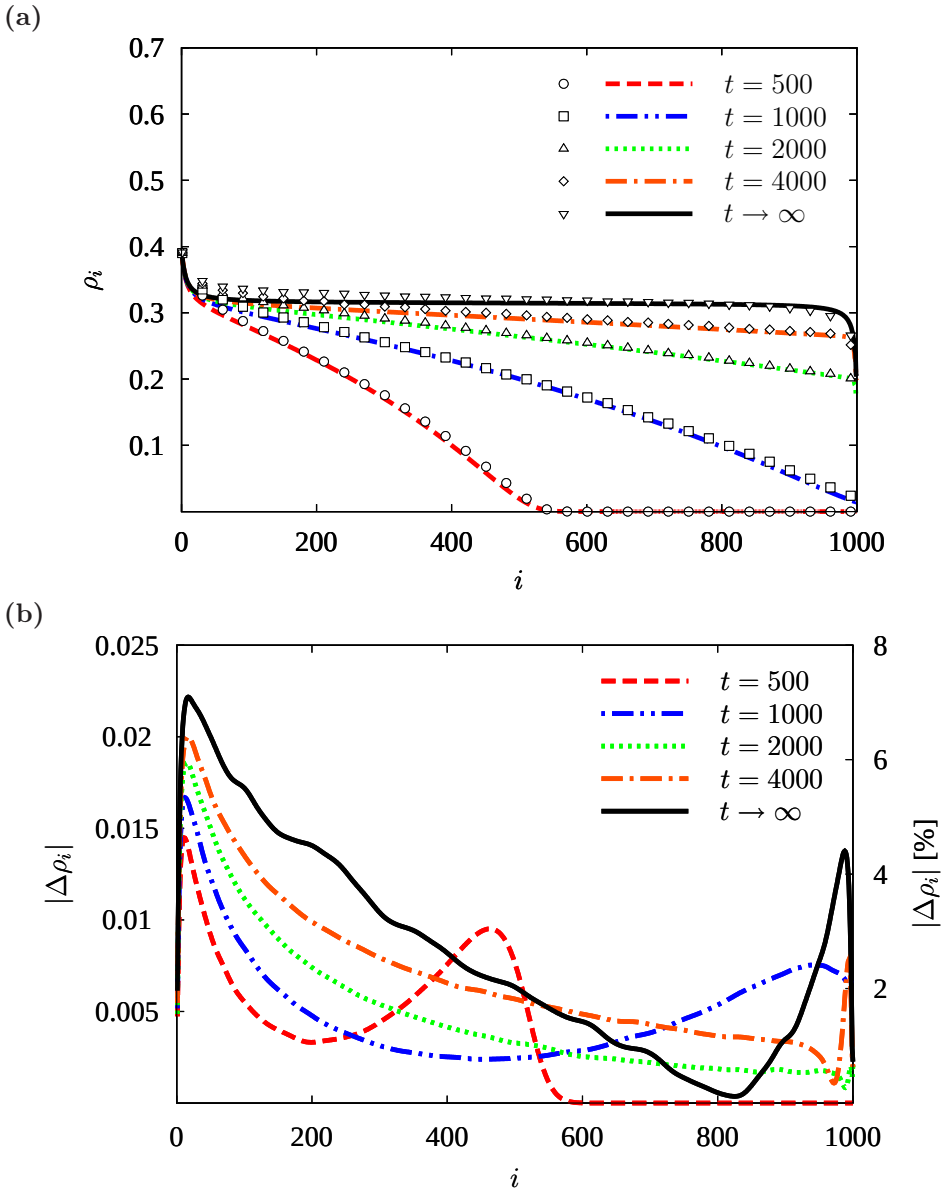

Figure 4.8: (a) Time evolution of a one-dimensional lattice gas corresponding to $V = 2V_c$. All other parameters are as in Fig. 4.7. (b) Here, the percentage is taken with respect to $\rho_B = \rho_1^*$.

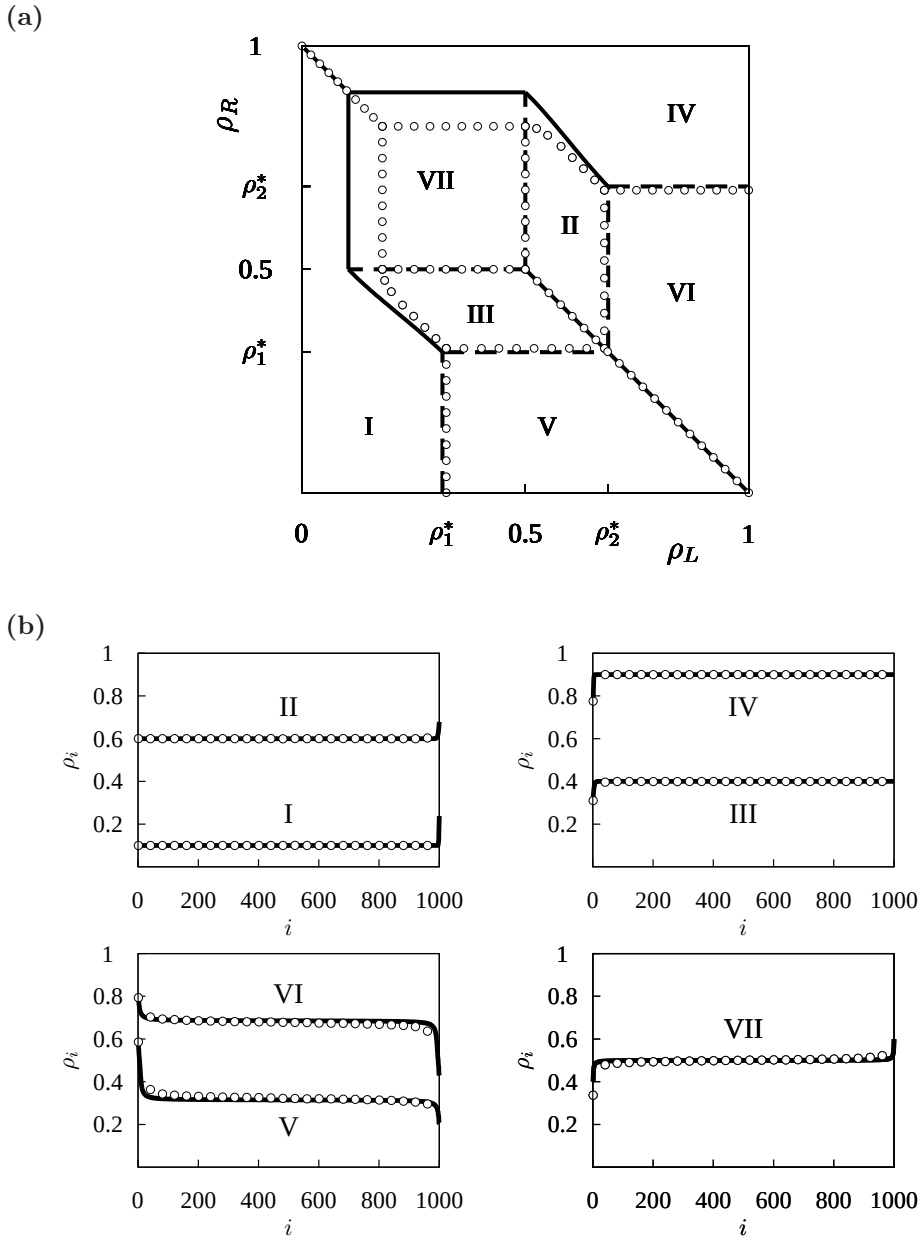

Figure 4.9: (a) Steady-state phase diagram and (b) density profiles of a system with 1000 sites and $V = 2V_c$. The phase diagram contains seven phases which are represented by density profiles corresponding to I ($\rho_B = \rho_L$, low-density phase): $\rho_L = 0.1$, $\rho_R = 0.4$; II ($\rho_B = \rho_L$): $\rho_L = 0.6$, $\rho_R = 0.7$; III ($\rho_B = \rho_R$): $\rho_L = 0.3$, $\rho_R = 0.4$; IV ($\rho_B = \rho_R$, high-density phase: $\rho_L = 0.6$, $\rho_R = 0.9$; V ($\rho_B = \rho_1^*$, maximal-current phase): $\rho_L = 0.6$, $\rho_R = 0.1$; VI ($\rho_B = \rho_2^*$, maximal-current phase): $\rho_L = 0.9$, $\rho_R = 0.4$; VII ($\rho_B = 0.5$, minimal-current phase): $\rho_L = 0.3$, $\rho_R = 0.7$. Solid and dashed lines in the phase diagram, which denote first- and second-order phase transitions, repsectively, as well as density profiles are calculated using TDFT. Data points are obtained by Monte Carlo simulations.

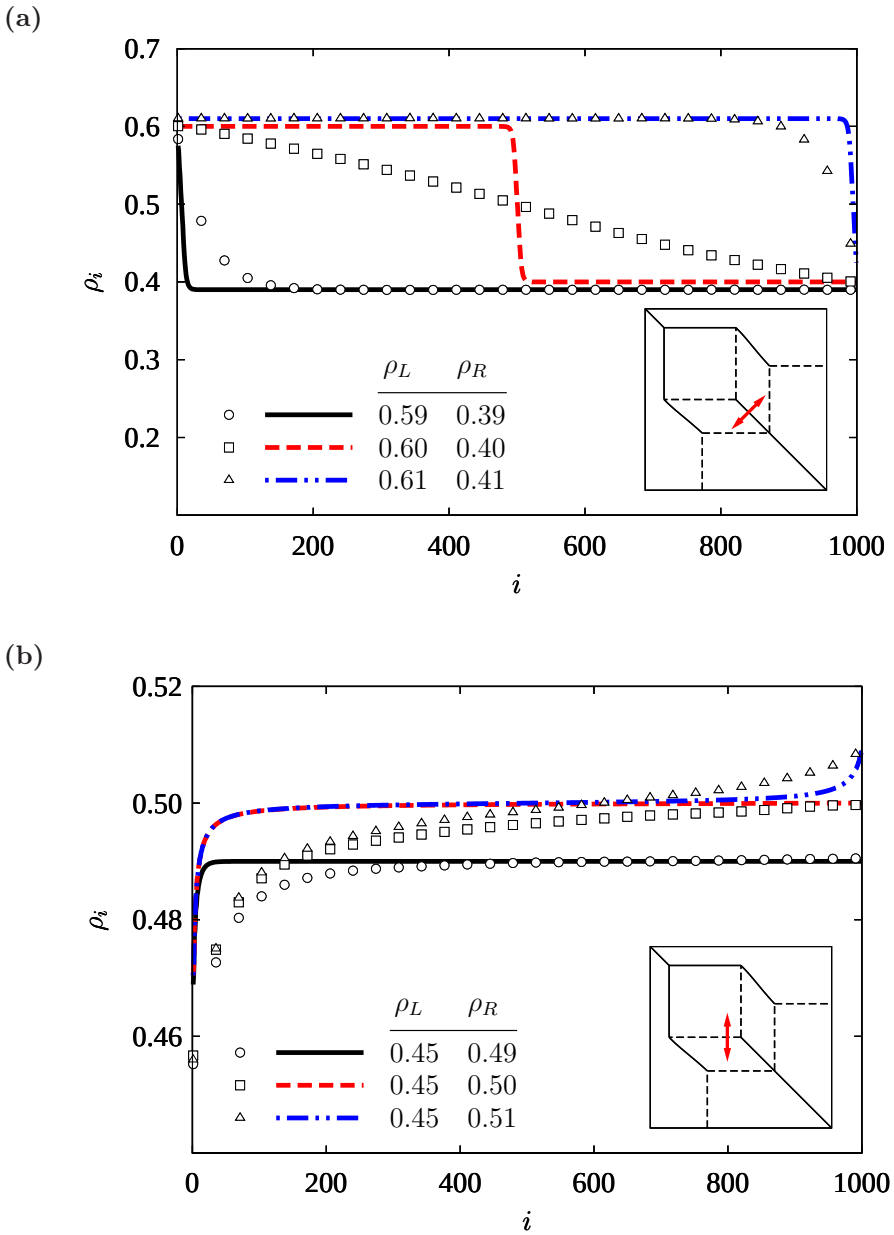

Figure 4.10: (a) First- and (b) second-order phase transition for a system of size $N = 1000$ and $V = 2V_c$. The plots include TDFT data (lines) as well as data from KMC simulations (symbols). The insets show the phase transitions in the phase diagram.

Chapter 5

Summary and outlook

In this work, the stochastic TASEP with short-range interactions is studied within a time-dependent DFT approach. Despite the simplicity of the model considered here, it allows a reliable investigation of transport processes which are important for many biological processes and nanotechnology devices. The main findings of this thesis are summarized as follows.

- An analytical expression for the current is derived. The analytical discussion shows that the particle flow for small V is increased as compared with the non-interacting case. A critical interaction strength V_c is also found, where the current reveals a double-hump structure with two maxima in $j(\rho)$ when V exceeds this value.

- Not only periodic systems can be studied by the TDFT formalism, but also systems with open boundaries. To demonstrate this, two distinct injection/extraction mechanisms are presented. In this context, it is shown that the behavior of the open system depends on the precise nature of the coupling mechanism and on the applied particle interactions. For purpose of theoretical investigations, constant profiles without non-universal boundary effects have proved to be successful.

- A microscopic description of the kinetics of phase changes is developed. To this end, solvable kinetic equations are established and solved numerically. This procedure yields the density profiles at all times. At long times, steady-state density profiles are obtained which are summarized in a density-parameterized phase diagram. It shows a complex phase behavior for $V > V_c$. More precisely, there are seven phases, separated by first- and second-order phase transitions.

Most of these TDFT findings agree on a quantitative level with KMC simulations. This is particularly true for weak and strong interparticle interactions. One can take this as an indication for the fundamental character of the TDFT formalism for systems driven out of thermal equilibrium.

Therefore, the advancement of this approach should be kept in mind. Particularly, it would be interesting to extend these TDFT studies to long-range Coulomb interactions by exploiting generalized Markov properties. This generalization is certainly a major step forward in order to treat charged particle transport through narrow channels. Introducing site energies can also be essential to approach more realistic systems. Examples are ion pumping driven by time-dependent site energies [ESDN10], photoelectric devices [REC09], and polaron formation on a molecular wire [GRN05].

Another attractive task would be to generalize the TDFT concept, explained in this thesis, to ASEP- and SSEP-like models. It is true that the TASEP plays a fundamental role for theoretical studies, but not in the framework of experimental setups applying finite bias voltages. Especially the symmetric exclusion process is of interest, because it offers methodologies for studying boundary driven systems in the absence of external fields.

Beside averaged currents calculated here, current fluctuations are observed in experimental investigations of charge-carrier transport. Following the studies of Prähofer and Spohn, the current fluctuations of the usual TASEP is a non-Gaussian of order $t^{1/3}$ [PS02]. However, for particle-particle interactions, there is less known about the scaling of fluctuations. Hence, their theoretical evaluation attracts wide interest.

An additional demanding task is to advance the classical idea of TDFT and particle hopping to the quantum regime. Much of modern devices operate at a scale, where quantum effects are significant. Despite the fact that efforts are being made to include quantum corrections in the classical concept, most quantum transport processes have been studied so far for lattice systems of non-interacting particles [HM09, LKHN02]. Thus, adding particle-particle interactions provides an interesting direction for future investigation.

More fundamental questions to be solved concern lattices in higher dimensions. Already in two dimensions, simulations of checkerboard lattices yield current functions with multiple maxima [Lei09]. But a reliable analytical theory regarding two- and higher-dimensional lattice gases with interparticle interactions is not available up to now. The presented TDFT approach could definitely be a promising candidate to close this gap.

Of course, the classical DFT is not able to paint a complete picture of non-equilibrium physics. Nevertheless, this theory is a powerful method for many driven systems and it is a well suited starting point for further studies in this domain.

Appendix A

Correlation functions in various systems

boundary conditions	**interaction strength**	**two-point correlator**
periodic	$V = 0$	$\langle n_i n_{i+1} \rangle = \langle n_i \rangle \langle n_{i+1} \rangle$
periodic	$V \neq 0$	$\langle n_i n_{i+1} \rangle \neq \langle n_i \rangle \langle n_{i+1} \rangle$
open	$V = 0$	$\langle n_i n_{i+1} \rangle \neq \langle n_i \rangle \langle n_{i+1} \rangle$ [1]
open	$V \neq 0$	$\langle n_i n_{i+1} \rangle \neq \langle n_i \rangle \langle n_{i+1} \rangle$

Table A: Characterization of correlation functions. The mean-field applicability is shown taking the example of the two-point correlation function for frequently used TASEP systems with stochastic update.

[1] Exact expressions for correlation functions are given in [DE93].

Appendix B

Transfer-matrix method

The transfer-matrix method is a strong instrument for solving problems in statistical mechanics. This part deals with a short guide on how a one-dimensional driven lattice gas with nearest-neighbor interactions can be solved by using this technique in combination with the equilibrium distribution of the Ising model.

The total energy of the Ising system for N spins and periodic boundaries is defined to be

$$\mathcal{H}(\mathbf{s}) = V \sum_{i=1}^{N} s_i s_{i+1} + h \sum_{i=1}^{N} s_i, \tag{B.1}$$

where $s_i = \{-1, 1\}$ is the ith spin, V denotes the coupling constant and h labels the external field. With expression (B.1), the partition function Z_N can be written in the form

$$Z_N = \sum_{s_1=\pm 1} \cdots \sum_{s_N=\pm 1} \prod_{i=1}^{N} \mathrm{e}^{-\beta\left[V s_i s_{i+1} + \frac{h}{2}(s_i + s_{i+1})\right]} = \mathrm{Tr}(T^N). \tag{B.2}$$

T is called 2×2 transfer matrix which is defined as

$$T = \begin{pmatrix} \mathrm{e}^{-V-h} & \mathrm{e}^{V} \\ \mathrm{e}^{V} & \mathrm{e}^{-V+h} \end{pmatrix} \tag{B.3}$$

to satisfy (B.2). Note that β has been absorbed in V and h. The two eigenvalues

$$\lambda_{\pm} = \mathrm{e}^{-V} \cosh h \pm \sqrt{\mathrm{e}^{2V} + \mathrm{e}^{-2V} \sinh^2 h} \tag{B.4}$$

of (B.3) determine Z_N as follows,

$$Z_N = \lambda_+^N + \lambda_-^N, \tag{B.5}$$

since the trace of T is the sum of its eigenvalues. Using Eq. (B.5), the averaged spin $\langle s \rangle$ at each site is given by

$$\langle s \rangle = -\lim_{N\to\infty} \frac{1}{N} \frac{\partial}{\partial h} \ln Z_N = -\frac{1}{\lambda_+} \frac{\partial}{\partial h} \lambda_+, \tag{B.6}$$

where the largest eigenvalue λ_+ dominates by applying the thermodynamic limit $N \to \infty$. Relating the averaged spin $\langle s \rangle \in [-1, 1]$ to the averaged site occupation $\langle n \rangle \in [0, 1]$ by $\langle s \rangle = 1 - 2\langle n \rangle$ and using Eqs. (B.4) and (B.6), $\langle n \rangle$ reads

$$\langle n \rangle = \frac{1}{2}\left(1 + \frac{\mathrm{e}^{-2V}\sinh h}{\sqrt{1 + \mathrm{e}^{-4V}\sinh^2 h}}\right). \tag{B.7}$$

Equation (B.7) determines the external field h for a given density $\langle n \rangle$. It is straightforward to derive higher-order correlation functions based on the transfer-matrix method. In particular, four-point correlators are required for computing the current in systems with nearest-neighbor interactions and TASEP dynamics. Appropriate expressions for them can be found in [HKPS01]. Because correlations obtained from this technique are valid in equilibrium, resulting non-equilibrium quantities like currents are in general not exact, but approximate expressions.

Appendix C

Equilibrium density correlations

The transfer-matrix method yields correlation functions having no spatial localization. Thus, it would be worthwhile to establish a procedure for deriving density functions with indices labeling the position on the lattice. To this end, consider a lattice system with total energy

$$\mathcal{H}(\mathbf{n}) = \sum_i \epsilon_i n_i + \frac{V}{2} \sum_{i \neq j} n_i n_j, \tag{C.1}$$

where n_i is the occupation number of site i, ϵ_i denotes the corresponding site energy and V labels the homogeneous interaction strength. In order to realize short-range interactions, the indices of the double sum satisfy the relation $|i - j| = 1$. The site energies in (C.1) are introduced to get a more generic lattice model and to show that they do not influence the resulting pair correlation function.

First of all, the joint probability of a microstate $\mathbf{n}$ is expressed by the Gibbs-Boltzmann formula on the one hand and on the other by a product of conditional probabilities as follows,

$$Z^{-1}\, \mathrm{e}^{-\mathcal{H}(\mathbf{n})} = P_{\mathrm{eq}}(n_1) \prod_{j=1}^{N-1} \Gamma(n_{j+1}|n_j), \tag{C.2}$$

where Z is the normalization factor, $P_{\mathrm{eq}}(n_1)$ is the equilibrium probability of the first of N occupation numbers and $\Gamma(n_{j+1}|n_j)$ labels the conditional probability. As before, the inverse thermal energy β was set equal to one for convenient notation. The conditional probabilities in (C.2) fulfill the Markov property due to the applied short-range interactions [Bus99].
In order to compute the equilibrium two-point correlation function, the following configurations are considered,

$$\mathbf{n} = \mathbf{0} \tag{C.3}$$

$$\mathbf{n} = \mathbf{0}, \text{ with the exception that } n_i = 1 \tag{C.4}$$

$$\mathbf{n} = \mathbf{0}, \text{ with the exception that } n_{i+1} = 1 \tag{C.5}$$

$$\mathbf{n} = \mathbf{0}, \text{ with the exception that } n_i = 1 \text{ and } n_{i+1} = 1. \tag{C.6}$$

After insertion of Eqs. (C.3)-(C.6) into (C.2), one has

$$Z^{-1} = (1-\rho_1)\prod_{j=1}^{N-1}\left(\frac{1-\rho_j-\rho_{j+1}+C_{j,j+1}}{1-\rho_j}\right) \tag{C.7}$$

$$Z^{-1}\,\mathrm{e}^{-\epsilon_i} = (1-\rho_1)\left(\frac{\rho_i-C_{i-1,i}}{1-\rho_{i-1}}\right)\left(\frac{\rho_i-C_{i,i+1}}{\rho_i}\right) \times \prod_{\substack{j=1\\ j\neq i-1,i}}^{N-1}\left(\frac{1-\rho_j-\rho_{j+1}+C_{j,j+1}}{1-\rho_j}\right) \tag{C.8}$$

$$Z^{-1}\,\mathrm{e}^{-\epsilon_{i+1}} = (1-\rho_1)\left(\frac{\rho_{i+1}-C_{i,i+1}}{1-\rho_i}\right)\left(\frac{\rho_{i+1}-C_{i+1,i+2}}{\rho_{i+1}}\right) \times \prod_{\substack{j=1\\ j\neq i,i+1}}^{N-1}\left(\frac{1-\rho_j-\rho_{j+1}+C_{j,j+1}}{1-\rho_j}\right) \tag{C.9}$$

$$Z^{-1}\,\mathrm{e}^{-(\epsilon_i+\epsilon_{i+1}+V)} = (1-\rho_1)\left(\frac{\rho_i-C_{i-1,i}}{1-\rho_{i-1}}\right)\left(\frac{C_{i,i+1}}{\rho_i}\right)\left(\frac{\rho_{i+1}-C_{i+1,i+2}}{\rho_{i+1}}\right) \times \prod_{\substack{j=1\\ j\neq i,i\pm1}}^{N-1}\left(\frac{1-\rho_j-\rho_{j+1}+C_{j,j+1}}{1-\rho_j}\right), \tag{C.10}$$

where the conditional probabilities have been replaced by use of Eq. (3.17). After some algebra, Eqs. (C.7)-(C.10) lead to the correlator equation [BMD00]

$$\mathrm{e}^{-V} = \frac{C_{i,i+1}(1-\rho_i-\rho_{i+1}+C_{i,i+1})}{(\rho_i-C_{i,i+1})(\rho_{i+1}-C_{i,i+1})}. \tag{C.11}$$

Expression (C.11) is a quadratic formula for the two-point correlator $C_{i,i+1}$, whose solution can be taken from Section 3.2.

Appendix D

Kinetic Monte Carlo method

Algorithm D: KMC($\mathbf{n}$, t_0, $t_{\max}$, $\Gamma_{i\to f}$)

remarks: This kinetic Monte Carlo (KMC) algorithm simulates the time evolution of a one-dimensional driven lattice gas from time t_0 to $t_{\max}$. The microstate of the system is stored in vector $\mathbf{n}$, where each lattice site j is either simply occupied ($n[\,j\,]=1$) or vacant ($n[\,j\,]=0$). At time t_0, $\mathbf{n}$ describes the initial configuration. The dynamics of the lattice gas is defined by $\Gamma_{i\to f}$, which is the hopping rate from initial site i to final site f. All possible jumps and their details (particle position, jump direction, time) are stored in the dynamic array **list**. To illustrate the implementation of measurement rules, the density ρ is measured on the first site.

$t_{\text{global}} \leftarrow t_0$
$T \leftarrow 0$
$\rho \leftarrow 0$
Find all possible hopping events and store position and hopping direction (± 1 for ASEP)
of the particles in $list[...].pos$ and $list[...].d$, respectively
$k \leftarrow list.size()$
for $j \leftarrow 1$ **to** k
do
- $i \leftarrow list[j].pos$
- $f \leftarrow list[j].pos + list[j].d$
- $list[j].t \leftarrow t_{\text{global}} - \frac{1}{\Gamma_{i\to f}} \ln(1-\sigma)$
- **comment:** σ is a uniformly distributed random number on the interval $[0,\,1[$.

while $t_{\text{global}} < t_{\max}$
do
- **comment:** Find jump at $t_{\min}$.
- $k \leftarrow list.size()$
- $t_{\min} \leftarrow \min(list[1].t,\, list[2].t, \ldots,\, list[k-1].t,\, list[k].t)$
- $i \leftarrow list[k_{\min}].pos$
- $f \leftarrow list[k_{\min}].pos + list[k_{\min}].d$
- **comment:** $k_{\min}$ is defined by $t_{\min} = list[k_{\min}].t$.
- **comment:** Measure density.
- $\Delta t \leftarrow t_{\min} - t_{\text{global}}$
- $T \leftarrow \Delta t + T$
- $\rho \leftarrow n[1]\Delta t + \rho$
- $t_{\text{global}} \leftarrow t_{\min}$
- **comment:** Perform selected jump at time $t_{\min}$, i.e., update $\mathbf{n}$.
- $n[i] \leftarrow 0$
- $n[f] \leftarrow 1$
- **comment:** Next, update **list**.
- Remove disabled jumps from **list**
- Insert enabled jumps (position, direction, time) into **list**
- Calculate new times for jumps, whose local configuration has been changed (if $\Gamma_{i\to f} = \Gamma_{i\to f}(\mathbf{n})$)
- **comment:** New times are generated as stated above.

output $(\frac{\rho}{T})$

References

[AS00] T. Antal and G. M. Schütz. Asymmetric exclusion process with next-nearest-neighbor interactions: Some comments on traffic flow and a non-equilibrium reentrance transition. *Physical Review E*, 62(1):83–93, 2000.

[BE07] R. A. Blythe and M. R. Evans. Nonequilibrium steady states of matrix-product form: a solver's guide. *Journal of Physics A*, 40(46):R333–R441, 2007.

[BGRS02] C. Bahadoran, H. Guiol, K. Ravishankar, and E. Saada. A constructive approach to Euler hydrodynamics for attractive processes. Application to k-step exclusion. *Stochastic Processes and their Applications*, 99(1):1–30, 2002.

[BKL75] A. B. Bortz, M. H. Kalos, and J. L. Lebowitz. A new algorithm for Monte Carlo simulation of Ising spin systems. *Journal of Computational Physics*, 17(1):10–18, 1975.

[BMD00] J. Buschle, P. Maass, and W. Dieterich. Exact density functionals in one dimension. *Journal of Physics A*, 33(4):L41–L46, 2000.

[Bus99] J. Buschle. Statistische Mechanik für eindimensionale Gittergase mit Randfeldern-exakte Ergebnisse. Master's thesis, University of Konstanz, 1999.

[DDM92] B. Derrida, E. Domany, and D. Mukamel. An exact solution of a one-dimensional asymmetric exclusion model with open boundaries. *Journal of Statistical Physics*, 69(3-4):667–687, 1992.

[DE93] B. Derrida and M. R. Evans. Exact correlation functions in an asymmetric exclusion model with open boundaries. *Journal de Physique I*, 3(2):311–322, 1993.

[DEHP93] B. Derrida, M. R. Evans, V. Hakim, and V. Pasquier. Exact solution of a 1D asymmetric exclusion model using a matrix formulation. *Journal of Physics A*, 26(7):1493–1517, 1993.

[Der98] B. Derrida. An exactly soluble non-equilibrium system: The asymmetric simple exclusion process. *Physics Reports*, 301(1-3):65–83, 1998.

[DFP80] W. Dieterich, P. Fulde, and I. Peschel. Theoretical models for superionic conductors. *Advances in Physics*, 29(3):527–605, 1980.

[EKMN10] M. Einax, M. Körner, P. Maass, and A. Nitzan. Nonlinear hopping transport in ring systems and open channels. *Physical Chemistry Chemical Physics*, 12(3):645–654, 2010.

[ESDN10] M. Einax, G. C. Solomon, W. Dieterich, and A. Nitzan. Unidirectional hopping transport of interacting particles on a finite chain. *Journal of Chemical Physics*, 133(5):054102, 2010.

[FRD+98] H. P. Fischer, J. Reinhard, W. Dieterich, J.-F. Gouyet, P. Maass, A. Majhofer, and D. Reinel. Time-dependent density functional theory and the kinetics of lattice gas systems in contact with a wall. *Journal of Chemical Physics*, 108(7):3028–3037, 1998.

[Gil76] D. T. Gillespie. A general method for numerically simulating the stochastic time evolution of coupled chemical reactions. *Journal of Computational Physics*, 22(4):403–434, 1976.

[Gil92] D. T. Gillespie. *Markov Processes: An Introduction for Physical Scientists*. Academic Press, 1992.

[GKCN04] P. Graf, M. G. Kurnikova, R. D. Coalson, and A. Nitzan. Comparison of dynamic lattice Monte Carlo simulations and the dielectric self-energy: Poisson-Nernst-Planck continuum theory for model ion channels. *Journal of Physical Chemistry B*, 108(6):2006–2015, 2004.

[GM06] O. Golinelli and K. Mallick. The asymmetric simple exclusion process: an integrable model for non-equilibrium statistical mechanics. *Journal of Physics A*, 39(41):12679–12705, 2006.

[GRN05] M. Galperin, M. A. Ratner, and A. Nitzan. Hysteresis, switching, and negative differential resistance in molecular junctions: a polaron model. *Nano Letters*, 5(1):125–130, 2005.

[GS92] L.-H. Gwa and H. Spohn. Bethe solution for the dynamical-scaling exponent of the noisy Burgers equation. *Physical Review A*, 46(2):844–854, 1992.

[HDMF04] S. Heinrichs, W. Dieterich, P. Maass, and H. L. Frisch. Static and time dependent density functional theory with internal degrees of freedom: Merits and limitations demonstrated for the Potts model. *Journal of Statistical Physics*, 114(3-4):1115–1125, 2004.

References

[Hel01] D. Helbing. Traffic and related self-driven many-particle systems. *Reviews of Modern Physics*, 73(4):1067–1141, 2001.

[HKPS01] J. S. Hager, J. Krug, V. Popkov, and G. M. Schütz. Minimal current phase and universal boundary layers in driven diffusive systems. *Physical Review E*, 63(5):056110, 2001.

[HM09] P. Hänggi and F. Marchesoni. Artificial Brownian motors: Controlling transport on the nanoscale. *Reviews of Modern Physics*, 81(1):387–442, 2009.

[Jar97] C. Jarzynski. Nonequilibrium equality for free energy differences. *Physical Review Letters*, 78(14):2690–2693, 1997.

[KLS84] S. Katz, J. L. Lebowitz, and H. Spohn. Nonequilibrium steady states of stochastic lattice gas models of fast ionic conductors. *Journal of Statistical Physics*, 34(3-4):497–537, 1984.

[KPZ86] M. Kardar, G. Parisi, and Y.-C. Zhang. Dynamic scaling of growing interfaces. *Physical Review Letters*, 56(9):889–892, 1986.

[Kru91] J. Krug. Boundary-induced phase transitions in driven diffusive systems. *Physical Review Letters*, 67(14):1882–1885, 1991.

[Lei09] D. Leipold. Classical transport in frustrated systems. Master's thesis, Technical University of Ilmenau, 2009.

[LKHN02] J. Lehmann, S. Kohler, P. Hänggi, and A. Nitzan. Molecular wires acting as coherent quantum ratchets. *Physical Review Letters*, 88(22):228305, 2002.

[LSZ89] K.-t. Leung, B. Schmittmann, and R. K. P. Zia. Phase transitions in a driven lattice gas with repulsive interactions. *Physical Review Letters*, 62(15):1772–1775, 1989.

[Löw94] H. Löwen. Melting, freezing and colloidal suspensions. *Physics Reports*, 237(5):249–324, 1994.

[Mer65] N. D. Mermin. Thermal properties of the inhomogeneous electron gas. *Physical Review*, 137(5A):1441 – 1443, 1965.

[MG69] C. T. MacDonald and J. H. Gibbs. Concerning the kinetics of polypeptide synthesis on polyribosomes. *Biopolymers*, 7(5):707–725, 1969.

[MN98] M. Matsumoto and T. Nishimura. Mersenne twister: A 623-Dimensionally equidistributed uniform pseudo-random number generator. *ACM Transactions on Modeling and Computer Simulation (TOMACS)*, 8(1):3–30, 1998.

[MS08] T. Mignot and J. W. Shaevitz. Active and passive mechanisms of intracellular transport and localization in bacteria. *Current Opinion in Microbiology*, 11(6):580–585, 2008.

[NDM93] M. Nieswand, W. Dieterich, and A. Majhofer. Density-functional method for lattice-gas problems. *Physical Review E*, 47(1):718–720, 1993.

[NR03] A. Nitzan and M. A. Ratner. Electron transport in molecular wire junctions. *Science*, 300(5624):1384–1389, 2003.

[NS92] K. Nagel and M. Schreckenberg. A cellular automaton model for freeway traffic. *Journal de Physique I*, 2(12):2221–2229, 1992.

[OJ98] K. Oerding and H. K. Janssen. Surface critical behavior of driven diffusive systems with open boundaries. *Physical Review E*, 58(2):1446–1454, 1998.

[Pri03] V. B. Priezzhev. Exact nonstationary probabilities in the asymmetric exclusion process on a ring. *Physical Review Letters*, 91(5):050601, 2003.

[PS99] V. Popkov and G. M. Schütz. Steady-state selection in driven diffusive systems with open boundaries. *Europhysics Letters*, 48(3):257–263, 1999.

[PS02] M. Prähofer and H. Spohn. *In and Out of Equilibrium*, chapter 7, pages 185–204. Birkhäuser, 2002.

[PS07] R. K. Pan and S. Sinha. Self-organization of price fluctuation distribution in evolving markets. *Europhysics Letters*, 77(5):58004, 2007.

[RD96] D. Reinel and W. Dieterich. Time-dependent density functional theory in lattice gas problems. *Journal of Chemical Physics*, 104(13):5234–5239, 1996.

[REC09] B. Rutten, M. Esposito, and B. Cleuren. Reaching optimal efficiencies using nanosized photoelectric devices. *Physical Review B*, 80(23):235122, 2009.

[Sch00] G. Schütz. *Phase Transitions and Critical Phenomena*, chapter 1, pages 1–251. Academic Press, 2000.

[SD93] G. Schütz and E. Domany. Phase transitions in an exactly soluble one-dimensional exclusion process. *Journal of Statistical Physics*, 72(1-2):277–296, 1993.

[Spi70] F. Spitzer. Interaction of Markov processes. *Advances in Mathematics*, 5(2):246–290, 1970.

Acknowledgment

Here I would like to take the opportunity to thank those people who spent their time and shared their knowledge for helping me to complete this thesis.

Particular thanks and gratitude go to my supervisor, Dr. Mario Einax, whose encouragement and assistance from the preliminary to the concluding level enabled me to develop an understanding of the subject. I would like to extend my thanks to Prof. Philipp Maaß, for introducing me to TDFT. Without his support this thesis would not have been possible.

Thanks also to the ever pleasant and helpful staff of Theoretical Physics I and II, who have made available their assistance in a number of ways.

I would like to make a special reference to my former fellow student Christiane Heinicke for proofreading.

Finally, an honorable mention goes to my family and friends for their understanding and support of me in completing this thesis. Without their help, I would have faced many difficulties while doing this work.

Ilmenau, September 2010 Marcel Dierl

Eidesstattliche Erklärung

Ich versichere hiermit, dass ich die vorliegende Arbeit mit dem Thema „One-dimensional hopping transport with nearest-neighbor interactions“ selbstständig verfasst und keine anderen Hilfsmittel als die angegebenen benutzt habe. Die Stellen, die anderen Werken dem Wortlaut oder dem Sinn nach entnommen sind, habe ich durch Angabe der Quellen kenntlich gemacht.

Ilmenau, den 24.09.2010

_____

(Unterschrift)